

ABSTRACT

Title of Thesis: SUBJECT-SPECIFIC MULTICHANNEL
BLIND SYSTEM IDENTIFICATION OF
HUMAN ARTERIAL TREE VIA CUFF
OSCILLATION MEASUREMENTS

Jongchan Lee, Master of Science, 2016

Thesis Directed By: Professor Jin-Oh Hahn
Department of Mechanical Engineering

We developed and evaluated a mathematical model-based method to monitor cardiovascular health and estimate risk predictors from two peripheral cuff oscillation measurements. The model structure was established by studying tube-load models individually augmented with a gain, Voigt model, and standard linear solid model to best capture the relationship between carotid tonometry and cuff waveforms at the upper arm and ankle. The arm-cuff interface was better modeled with increasing viscoelasticity but not as much for the ankle-cuff interface. Next, model-estimated ankle blood pressure waveforms were used to formulate a matrix equation for estimating wave reflection. Subsequently derived risk predictors were adequately correlated with those from reference methods. Finally, subject-specific central blood pressure waveforms were estimated from two cuff oscillation signals via multichannel blind system identification. The model estimated central arterial blood pressure waveforms with good accuracy with a median RMSE of 3.08 mmHg and IQR of 1.71 mmHg.

SUBJECT-SPECIFIC MULTICHANNEL BLIND SYSTEM IDENTIFICATION OF
HUMAN ARTERIAL TREE VIA CUFF OSCILLATION MEASUREMENTS

by

Jongchan Lee

Thesis submitted to the Faculty of the Graduate School of the
University of Maryland, College Park, in partial fulfillment
of the requirements for the degree of
Master of Science
2016

Advisory Committee:
Professor Jin-Oh Hahn, Chair
Professor Balakumar Balachandran
Professor Nikhil Chopra

© Copyright by
Jongchan Lee
2016

Acknowledgements

First and foremost, I would like to thank Dr. Hahn for accepting me into his lab. His continuous support and guidance are the main reason I was able to complete this work. I truly appreciate his time and efforts in challenging me to become a better student and critical thinker. I wish that my research can lead to larger discoveries for Dr. Hahn and the rest of the lab.

Also, my colleagues in the lab deserve recognition, especially Dr. Chang-Sei Kim and Zahra Ghasemi. Throughout my two years, they have made themselves available for assistance and this work would not have been possible without their help.

Next, thank you to Prof. Ramakrishna Mukkamala and his group from Michigan State University. He has provided much insight and advice from his extensive experience in modeling the cardiovascular system.

This work also would not have been possible without Prof. Chen-Huan Chen of National Yang Ming University and Profs. Hao-Min Cheng and Shih-Hsien Sung of Taipei Veterans General Hospital in Taipei, Taiwan. They have provided us with archived data of over 700 subjects, many of which were used for this work. They have also guided our work with their experience and expertise in the medical field.

My sincere thanks and gratitude go to Profs. Balakumar Balachandran and Nikhil Chopra for agreeing to be on my thesis committee. I truly appreciate your contributions in the classroom and your advice on this work.

I would like to thank the NSF for the financial support of this work under grants IIS-1404436 and IIS-1403004. This work would not have been possible without funding.

Finally and most importantly, I would like to thank my parents, sister, and friends. Their unconditional love and support gave me the strength to push through my trials and tribulations and I look forward to sharing my success with everyone.

Table of Contents

Acknowledgements.....	ii
Table of Contents	iv
List of Tables	vi
List of Figures	vii
List of Abbreviations	viii
Chapter 1: Introduction	1
1.1 Importance of Cardiovascular Health Monitoring	1
1.2 Established Cardiovascular Disease Risk Factors	1
1.3 Techniques for Cardiovascular Health Monitoring	4
1.4 Review of Model-Based Estimation of Risk Factors.....	5
1.4.1 Estimation of Central Arterial Blood Pressure	5
1.4.2 Multichannel Blind System Identification	6
1.4.3 Quantification of Wave Reflection	8
1.5 Thesis Goal and Outline.....	8
Chapter 2: Characterization of the Relationship between Carotid Tonometry and Distal Pulse Volume Recordings	10
2.1 Introduction to the Tube-Load Viscoelastic Models	10
2.2 Mathematical Formulation of Tube-Load Viscoelastic Models	11
2.2.1 Tube-Load Model Transfer Function.....	11
2.2.2 Tube-Load Viscoelastic Model Transfer Functions	12
2.2.3 Discretization	13
2.3 Identifiability Analysis.....	14
2.4 Data Set.....	15
2.5 Model Optimization via System Identification.....	18
2.6 Results.....	19
2.6.1 Estimation of Carotid Arterial Blood Pressure	19
2.6.2 Frequency Response Results.....	22
2.6.3 Akaike Information Criterion	25
2.7 Discussion.....	25
2.7.1 Relationship between Central Aortic BP and Distal PVR.....	25
2.7.2 Limitations	26
Chapter 3: Wave Reflection Quantification Using Estimated Central and Peripheral Blood Pressure Waveforms	28
3.1 Problem Formulation	28
3.2 Data Set.....	29
3.3 Methods.....	30
3.4 Results.....	31
3.5 Discussion.....	35
Chapter 4: Two-Sensor Blind System Identification	37
4.1 Introduction to Individualized Transfer Functions	37
4.2 Model of Human Arterial Tree	38
4.3 Mathematical Formulation of Blind System Identification Problem.....	39

4.4	Identifiability Analysis.....	40
4.5	Model Optimization.....	41
4.6	Data Sets	42
4.7	Results.....	43
4.6.1	Model Selection (Testing Set)	43
4.6.3	Comparison with State-of-the-Art (Validation Set).....	49
4.8	Discussion.....	50
Chapter 5: Conclusions and Future Directions		52
Appendix.....		54
Bibliography		61

List of Tables

- Table 1.1: Summary of reported models
- Table 2.1: Model identification subject characteristics
- Table 2.2: TLVE error results
- Table 2.3: Optimal model parameters associated with TLG, TLV, and TLS models
- Table 2.4: Akaike information criterion
- Table 3.1: Wave reflection subject characteristics
- Table 3.2: Reference and estimated CV risk predictors
- Table 3.3: Correlations between reference and estimated CV risk predictors
- Table 4.1: Blind model identification subject characteristics
- Table 4.2: Objective functions tested to reduce DBP error
- Table 4.3: DP error incorporation results
- Table 4.4: Final set of candidate objective functions
- Table 4.5: Results of final candidate objective functions
- Table 4.6: Verification of identifiability conditions (testing set)
- Table 4.7: Comparison of ITF-4 and current standards on validation set
- Table 4.8: Verification of identifiability conditions (validation set)
- Table A1: Individual results for test set
- Table A2: Individual results for ITF-4 on validation set

List of Figures

Fig. 2.1: A mechanistic model employed to relate carotid artery tonometry waveform to a distal pulse volume waveform (PVR)

Fig. 2.2: Examples of conditions for exclusion of data

Fig. 2.3: Representative example of measured ($P_p(k)$) and model-predicted ($\hat{P}_p(k, \theta^*)$) carotid artery tonometry waveform as well as measured pulse volume waveform (PVR) ($P_c(k)$)

Fig. 2.4: Bland-Altman plots associated with carotid SP, DP, and PP in all subjects

Fig. 2.5: Frequency responses associated with TLG, TLV, and TLS models

Fig. 3.1: An example of wave decomposition, with reconstruction of ABP waveforms

Fig. 3.2: Correlation and Bland-Altman plots associated with PTT, $|P_f(t)|$, $|P_b(t)|$, RM and RI

Fig. 4.1: Schematic of human arterial tree from Reymond, *et al.*

Fig. 4.2: Two-sensor cuff model

Fig. 4.3: Representative result of (4.8)

List of Abbreviations

- ABP – arterial blood pressure
- AIC – Akaike information criterion
- BP – blood pressure
- CO – cardiac output
- CV – cardiovascular
- CVD – cardiovascular disease
- PWV – pulse wave velocity
- PTT – pulse transit time
- SBP – systolic blood pressure
- DBP – diastolic blood pressure
- GTF – generalized transfer function
- ITF – individualized transfer function
- PP – pulse pressure
- PVR – pulse volume recording
- RI – reflection index
- RM – reflection magnitude
- SLS – standard linear solid
- TL – tube-load model
- TLG – tube-load model augmented by a gain
- TLS – tube-load model augmented by a SLS model
- TLV – tube-load model augmented by a Voigt model
- TLVE – tube-load model augmented by a viscoelastic model

Chapter 1: Introduction

1.1 Importance of Cardiovascular Health Monitoring

In the United States cardiovascular diseases (CVD), including but not limited to stroke, atherosclerosis, and heart failure, are the leading causes of death in the world. According to the American Heart Association, CVD were responsible for more than 800,000 deaths in 2013, roughly 30% of all deaths in the United States [1]. Although death rates linked to CVD decreased by 28.8% from 2003 to 2013, it remains very high at an average of 1 American death every 40 seconds. In addition 20% of CVD-related deaths occurred before the age of 65 and 35% before 75, highlighting the urgent need for early detection, prevention, and/or treatment.

Linked with the number of CVD cases, the associated costs were high as well. For 2011 to 2012, healthcare costs accounted for an estimated \$193.1 billion, greater than double of the direct costs associated with cancer. Indirect costs, such as lost future productivity, were estimated to be \$125 billion contributing to a total cost of more than \$316 billion. In order to reduce mortality rates and costs associated with CVD, clinicians utilize established techniques to diagnose risks of developing CVD, but these methods have room for improvement.

1.2 Established Cardiovascular Disease Risk Factors

CVD risk factors are certain characteristics of the cardiovascular (CV) system that are linked to increased risks of developing a CVD. One property of particular interest is the arterial blood pressure (ABP) wave propagation and reflection phenomena. In

summary, the ABP at any point in the arterial tree is the superposition of the forward wave created by the ejection from the heart and the backward wave traveling back to the heart after it is reflected at the peripheral vascular beds [2]–[5]. Wave reflection can be utilized in different ways to assess different aspects of the CV system such as cardiac afterload and arterial stiffness.

Arterial stiffness can also be assessed by pulse wave velocity (PWV), which is the speed of the ABP waveform as it propagates through the arterial tree [6], [7]. Increased wave reflection is a significant contributor of increased arterial stiffness and early vascular aging [8]–[11]. An alternative to PVW is pulse transit time (PTT), the time it takes for an ABP waveform to travel a certain distance. PWV can be estimated from PTT by dividing the distance between two points divided the PTT between the same two points.

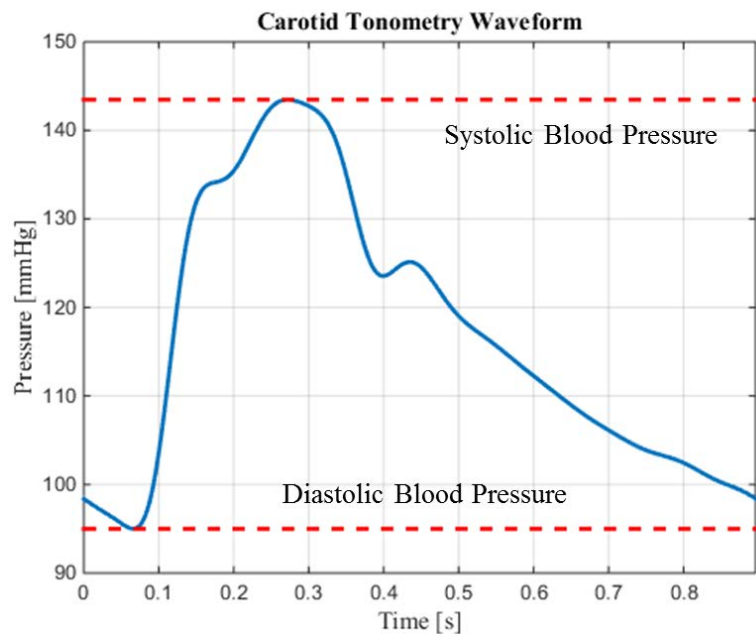


Fig. 1.1: Example of a hypertensive subject.

One estimate of wave reflection is hypertension. Hypertension is defined as elevated systolic blood pressure (SBP) and diastolic blood pressure (DBP), specifically

higher than 140 mmHg and 90 mmHg, respectively. As wave reflection increases, a backward wave of greater amplitude combines with the forward wave, increasing the overall ABP [12]–[14]. In some studies, increased wave reflection has been shown to be linked with age-dependent increase in SBP and DBP [8], [9]. Hypertension is one of the most commonly used risk factors because it can be easily measured using publicly available BP cuff machines, albeit with limited accuracy. As shown in Fig. 1.1 a hypertensive patient has a SBP of higher than 140 mmHg and/or diastolic DBP higher than 90 mmHg, compared to ideal blood pressures of 120 mmHg and 80 mmHg, respectively. Hypertension increases the afterload on the heart, the minimum pressure needed to eject blood from the heart, which reduces the cardiac output (CO) and strains the CV system [11]. The difference of SBP and DBP, pulse pressure (PP), is another measure of CV health. In multiple studies higher PP was associated with increased mortality [15]–[18] and in others, lower PP was associated with increased mortality as well [19], [20]. Wave reflection can also be explicitly quantified by reflection magnitude (RM) and reflection index (RI), which are defined by:

$$RM = \frac{|P_b|}{|P_f|}, \quad RI = \frac{|P_b|}{|P_f| + |P_b|}$$

where $|P_f|$ and $|P_b|$ are PP of forward and backward ABP waves, respectively [21], [22].

Traditionally, clinicians have measured blood pressure by wrapping around the brachial artery at the upper arm with an inflated sphygmomanometer (BP cuff) and listening for the Korotkoff sounds using a stethoscope due to the ease and accessibility of measuring ABP at the arm. However, the ABP waveform morphology becomes increasingly distorted, typically observed as pulse pressure amplification, as it travels along the arterial tree [23], and central CVD risk predictors were shown to have more

clinical value than those measured at peripheral locations [15], [24]–[29]. Despite the added reliability of the central CVD risk predictors, most have not been incorporated into routine clinical practice due to difficulties in obtaining accurate measurements.

1.3 Techniques for Cardiovascular Health Monitoring

The measurement of central ABP waveforms is a nontrivial issue because the techniques available today are invasive, costly, and require a trained expert to operate the device. The current gold standard for measuring central ABP is aortic catheterization which involves inserting a thin, flexible wire equipped with a pressure sensor into the femoral (upper thigh) or radial (forearm) arteries. While the accuracy of aortic catheterization is unrivaled, it is an unnecessary procedure in routine clinical settings due to its invasive nature and nontrivial process.

As a result, carotid artery tonometry has been widely adopted as a noninvasive alternative [30]–[32]. Applanation tonometry requires a trained operator to applanate, or to flatten, the artery of interest against the surrounding tissue and bones [30], [33]. Tonometry also allows for measurement of distal ABP waveforms, typically at the femoral and radial arteries, but the need for an expert to perform the measurements deters the implementation into daily practice.

To bypass specialized techniques such as catheterization and tonometry, pulse volume waveform, also called pulse volume recording (PVR), has been investigated in an effort to exploit the easily measured signal by calibrating the PVR waveform using ABP values estimated via brachial oscillometry [34]–[37]. Obtained using a blood pressure (BP) cuff, PVR is the small-amplitude oscillation of the pressure in the cuff as a result of ABP pulsation coupled by arterial vessel-tissue-cuff bladder mechanics [38], [39].

Additionally the morphology of PVR waveforms is similar to that of ABP waveforms. Accommodated by the simple procedure, PVR offers opportunities for implementation of improved methods of CV health monitoring into daily practice.

1.4 Review of Model-Based Estimation of Risk Factors

1.4.1 Estimation of Central Arterial Blood Pressure

The introduction of noninvasive ABP measurements such as applanation tonometry and PVR has led to the development of mathematical techniques to derive central ABP waveforms from a noninvasive distal measurement and subsequently quantify wave reflection and other CVD risk factors. Most of the current methods estimate central ABP by a generalized transfer function (GTF). A GTF is a population-based transfer function optimized by using proximal and distal ABP measurements, such as carotid tonometry and brachial PVR, from a set of subjects. The transfer function is then applied to distal ABP measurements from a new set of subjects [40]–[48] to estimate central ABP. There are various types of GTFs, but frequency response-based models, physiology-based models, and regression models are among the most common. The appeal of GTF is the relative ease of application; once the model is compiled it can estimate central ABP from only one distal measurement.

However, GTFs lack adaptability as it is impossible to account to individual differences between subjects. As a result, individualized transfer functions (ITF) have been developed and reviewed to account for inter-subject variability [49]–[56]. In many of these reports, the tube-load (TL) model (Fig. 1.2) has been incorporated to exploit the wave reflection phenomena incorporated into the transfer function, which when applied to invasively measured or tonometry measured ABP waveforms, accurately reproduced

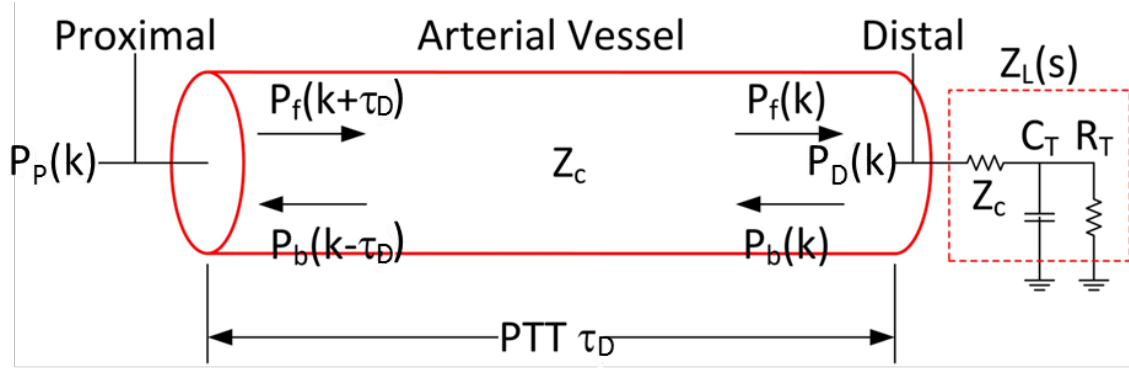


Fig. 1.2: Lossless Windkessel load tube-load model. $P_i(k)$: proximal ABP. $P_o(k)$: distal ABP. $P_f(k)$: forward ABP wave. $P_b(k)$: backward ABP wave. Z_c : tube characteristic impedance. Z_L : terminal load impedance (Windkessel load).

central ABP waveforms [49]–[56]. Recently, methods of estimating central ABP from peripheral PVR waveforms, typically at the brachial artery, utilizing GTFs representing the relationship have been reported and validated [34], [37], [46]–[48], [57], [58]. As was the case previously, the systematic inability to personalize the process leaves much room for improvement. Table 1.1 summarizes the techniques listed above.

1.4.2 Multichannel Blind System Identification

Blind system identification is a signal processing technique used to identify a system’s unknown properties or input from its output only. Similarly, multichannel blind system identification (MBSI) estimates the system and/or its input(s) from the outputs of each channel. Investigations have shown that a single-input and multiple-output (SIMO) system can be characterized via MBSI techniques by placing sensors at the output locations [59], [60]. Though mainly used in communications or image processing, preliminary studies have shown that the MBSI methodology can be directly applied to the cardiovascular system by measuring BP waves at two distinct peripheral locations (e.g arm and leg) in order to identify the system dynamics [50], [51], [55].

Table 1.1: Summary of reported models

Author (year)	Proximal Measurement Method	Distal Measurement Method	Class of Transfer Function	Reference
Karamanoglu (1993)	Aortic Cath.	1) Brachial Cath. 2) Radial Cath.	GTF	[40]
Fetics (1999)	Aortic Cath.	Radial Tonometry	GTF	[41]
Pauca (2001)	Aortic Cath.	Radial Cath.	GTF	[42]
Söderström (2002)	Aortic Cath.	Radial Cath.	GTF	[43]
Gallagher (2004)	Carotid Tonometry	Radial Tonometry	GTF	[44]
Sharman (2006)	Aortic Cath.	Radial Tonometry	GTF	[45]
Cheng (2010)	Aortic Cath.	1) Brachial Cath. 2) Brachial Oscill.	GTF	[46]
Weber (2011)	Aortic Cath.	1) Brachial Oscill. 2) Radial Tonometry	GTF	[47]
Shih (2013)	Aortic Cath.	1) Brachial Cath. 2) Brachial Oscill.	GTF	[48]
Swamy (2007)	N/A	1) Femoral Cath. 2) Brachial Cath.	ITF	[49]
Hahn (2009)	Aortic Cath.	1) Femoral Cath. 2) Radial Cath.	ITF	[50]
Swamy (2009)	Aortic Cath.	Femoral Cath.	ITF	[52]
Hahn (2012)	Aortic Cath.	Radial Cath.	ITF	[53]
Rashedi (2013)	Aortic Cath.	1) Femoral Cath. 2) Radial Cath.	ITF	[54]
Fazeli (2014)	Aortic Cath.	1) Femoral Cath. 2) Radial Cath.	ITF	[55]
Abdollahzade (2014)	Aortic Cath.	1) Femoral Cath. 2) Radial Cath.	ITF	[56]
Wassertheurer (2010)	N/A	Brachial Oscill.	GTF	[57]
Climie (2012)	N/A	Brachial PVR	GTF	[34]
Brett (2012)	N/A	Brachial PVR	GTF	[58]
Verberk (2016)	N/A	Brachial PVR	GTF	[37]

1.4.3 Quantification of Wave Reflection

The breadth of importance of wave reflection across multiple CVD risk factors make it an attractive platform for developing techniques to estimate the dynamics of reflection. As such, a variety of methods have been reported ranging from measurement-based methods [21], [61], [62] to model-based methods [2], [7], [63]–[66]. Measurement-based methods extract information from measured data, such as differences in ABP waveform before and after occlusion of a distal artery [21] or subtle characteristics of the ABP waveform [62], in order to estimate forward and backward BP waves. Model-based methods utilize estimated values of parameters such as PTT and reflection coefficient (Γ) or estimated central ABP waveforms to calculate the corresponding forward and backward waves.

1.5 Thesis Goal and Outline

The objective is to develop an easy to use, innovative, individualized, low cost, and noninvasive method for estimating central ABP and subsequently extract CVD risk factors. This method utilizes peripheral PVR measurements at the upper arm (brachial artery) and ankle (posterior-tibial artery) to derive the central ABP. First, in Chapter 2, candidate models to represent the relationship between brachial PVR and central ABP and the relationship between ankle PVR and central ABP are studied and compared with the TL model, an established ITF for use with invasive or high-fidelity tonometry waveforms. Chapter 3 estimates wave reflection by decomposing the model estimated central ABP waveform and ankle PVR into forward and backward BP waves. The decomposed waves and the extracted CVD risk factors are compared to those obtained from carotid tonometry and femoral (upper thigh) tonometry waveforms, which is treated

as the reference. Theoretically, the two methods should agree well with each other since the femoral and posterior-tibial arteries are part of the same branch in the arterial tree. Finally, Chapter 4 identifies the noninvasive 2-sensor individualized arterial tree model which is compared to and an existing, standard noninvasive 1-sensor GTF.

Chapter 2: Characterization of the Relationship between Carotid Tonometry and Distal Pulse Volume Recordings

2.1 Introduction to the Tube-Load Viscoelastic Models

To investigate the relationship between carotid artery tonometry and the distal PVR waveforms (at the brachial and posterior-tibial arteries) the candidate models were first developed starting from the TL model due to its physical basis and inherent ability to account to for the wave propagation phenomena. As shown in Fig. 2.1, a viscoelastic model, which represents the lumped dynamic pressure-volume relationship of the arterial wall, tissues, and BP cuff bladder, was connected in series with the TL model (Fig. 1.2) to form a tube-load viscoelastic model (TLVE). The TL model relates distal ABP, P_D , to proximal ABP, P_P , and the viscoelastic model relates cuff pressure, P_C , to P_D . Three models of varying viscoelasticity were employed to assess the relationship between the central and distal measurements.

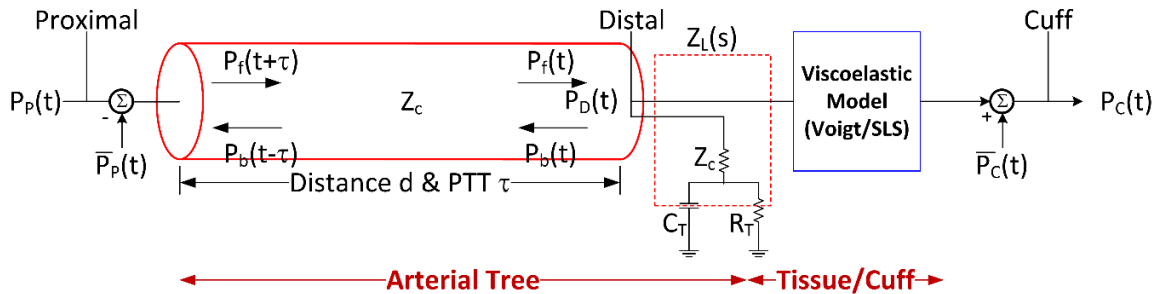


Fig. 2.1: A mechanistic model employed to relate carotid artery tonometry waveform to a distal pulse volume waveform (PVR). The model is composed of a tube-load (TL) model representing the arterial blood pressure (ABP) wave propagation and reflection in the artery and a viscoelastic model representing the lumped, dynamic pressure-volume relationships of the arterial wall, tissues, and BP cuff. $P_P(t)$: Proximal ABP (carotid artery tonometry waveform). $P_D(t)$: Distal ABP. $P_C(t)$: PVR.

1. TLG: TL model augmented with a constant, purely elastic, gain to represent a relationship between proximal and distal waveforms that is dominated by wave reflection
2. TLV: TL model augmented with a Voigt model, a well-known viscoelastic model, to represent a relationship that combines wave reflection and viscoelasticity
3. TLS: TL model augmented with a standard linear solid (SLS) model, a more complex viscoelastic model

2.2 Mathematical Formulation of Tube-Load Viscoelastic Models

2.2.1 Tube-Load Model Transfer Function

The TL model is characterized by the terminal load impedance, Z_L , and reflection coefficient, Γ . The terminal load impedance of the Windkessel load is given by

$$Z_L(s) = Z_C + \frac{R_T}{R_T C_T s + 1} \quad (2.1)$$

where s is the Laplace variable, Z_C is the characteristic impedance, and R_T and C_T are the peripheral resistance exerted by the arterioles and compliance of distant arteries,

respectively. $Z_C = \sqrt{\frac{l_L}{c_L}}$ is a constant due to constant inertance, l_L , and compliance, c_L ,

following the Bramwell-Hill equation. The terminal load impedance is formulated such that the impedance depends on the frequency of the signal and $Z_L = Z_C$ when $s = 0$ [65].

The reflection coefficient, defined as the mismatch between the tube and terminal impedances, is given by

$$\Gamma(s) = \frac{Z_L(s) - Z_C}{Z_L(s) + Z_C} = \frac{R_T}{2Z_C R_T C_T s + (2Z_C + R_T)} \quad (2.2)$$

Finally, the relationship between proximal and distal ABP can be formulated as

$$P_P(s) = G(s)P_D(s) = \frac{1 + \Gamma(s)}{e^{\tau s} + e^{-\tau s}\Gamma(s)} P_D(s) \quad (2.3)$$

following the transmission line theory [67], [68], and by substituting (2.2) into (2.3) the transfer function is expressed as

$$P_P(s) = \frac{s + \theta_1 + \theta_2}{(s + \theta_1)e^{\tau s} + \theta_2 e^{-\tau s}} P_D(s) \quad (2.4)$$

where

$$\tau \text{ is PTT, } \theta_1 = \frac{2Z_C + R_T}{2Z_C R_T C_T}, \text{ and } \theta_2 = \frac{R_T}{2Z_C R_T C_T}. \quad (2.5)$$

2.2.2 Tube-Load Viscoelastic Model Transfer Functions

In addition to the TL model, the viscoelastic models provide the relationship between distal ABP and PVR. Among the three proposed viscoelastic models, the gain model is given by

$$P_C(s) = \frac{1}{E_1} P_D(s) \quad (2.6)$$

where E_1 is the elastic coefficient. This model dictates that PVR is simply a scaled form of the distal ABP. The Voigt model is expressed as

$$P_C(s) = \frac{1}{E_1 + \eta s} P_D(s) \quad (2.7)$$

where E_1 and η the elastic and damping coefficients associated with a spring and dashpot connected in parallel. Finally, the SLS model is given by

$$P_C(s) = \frac{E_2 + \eta s}{E_1 E_2 + (E_1 + E_2)\eta s} P_D(s) \quad (2.8)$$

where η and E_2 are the damping and elastic coefficients of the dashpot and spring connected in series, and E_1 is the elastic coefficient of the spring connected in parallel with the spring and dashpot. It can be seen from equations (2.6)-(2.8) that the gain model is a specific case of the Voigt model when $\eta = 0$, and the Voigt model is a special case of the SLS model when $E_2 = \infty$.

Combining the TL model transfer function with those of the viscoelastic models results in the three physical models under investigation: TLG model (2.9a), TLV model (2.9b), and TLS model (2.9c).

$$P_C(s) = \frac{1}{E_1} P_D(s) = \frac{1}{E_1} \frac{s + \theta_1 + \theta_2}{e^{\tau s}(s + \theta_1) + e^{-\tau s}\theta_2} P_P(s) \quad (2.9a)$$

$$P_C(s) = \frac{1}{E_1 + \eta s} P_D(s) = \frac{1}{E_1 + \eta s} \frac{s + \theta_1 + \theta_2}{e^{\tau s}(s + \theta_1) + e^{-\tau s}\theta_2} P_P(s) \quad (2.9b)$$

$$\begin{aligned} P_C(s) &= \frac{E_2 + \eta s}{E_1 E_2 + (E_1 + E_2)\eta s} P_D(s) \\ &= \frac{E_2 + \eta s}{E_1 E_2 + (E_1 + E_2)\eta s} \frac{s + \theta_1 + \theta_2}{e^{\tau s}(s + \theta_1) + e^{-\tau s}\theta_2} P_P(s) \end{aligned} \quad (2.9c)$$

2.2.3 Discretization

As illustrated in Fig. 2.1, the TLVE models in (2.9a)-(2.9c) were applied to detrended waveforms to minimize artifacts caused by the DC components. Therefore, the discretized models only utilize the pulsatile components, $\tilde{P}_X(t) = P_X(t) - \bar{P}_X(t)$, where $\bar{P}_X(t)$ is the mean value of $P_X(t)$. Using the forward difference approximation, $s \approx F_S(z - 1)$ [69], where F_S is the sampling frequency (250 Hz) and z is the forward shift operator, the discretized models are as follows: TLG model (2.10a), TLV model (2.10b), and TLS model (2.10c).

$$\begin{aligned} \tilde{P}_P(k+1) &= \left(1 - \frac{\theta_1 + \theta_2}{F_S}\right) \cdot \tilde{P}_P(k) + E_1 \cdot \tilde{P}_C(k + \Delta + 1) + E_1 \left(\frac{\theta_1}{F_S} - 1\right) \cdot \tilde{P}_C(k + \Delta) \\ &\quad + \frac{\theta_2 E_1}{F_S} \cdot \tilde{P}_C(k - \Delta) \end{aligned} \quad (2.10a)$$

$$\begin{aligned} \tilde{P}_P(k+1) &= \left(1 - \frac{\theta_1 + \theta_2}{F_S}\right) \cdot \tilde{P}_P(k) + \eta F_S \cdot \tilde{P}_C(k + \Delta + 2) + (E_1 + \theta_1 \eta - 2\eta F_S) \\ &\quad \cdot \tilde{P}_C(k + \Delta + 1) + \left(\frac{\theta_1 E_1}{F_S} - E_1 - \theta_1 \eta + \eta F_S\right) \cdot \tilde{P}_C(k + \Delta) + \theta_2 \eta \\ &\quad \cdot \tilde{P}_C(k - \Delta + 1) + \left(\frac{\theta_2 E_1}{F_S} - \theta_2 \eta\right) \cdot \tilde{P}_C(k - \Delta) \end{aligned} \quad (2.10b)$$

$$\begin{aligned}
\tilde{P}_p(k+1) = & \left(2 - \frac{\theta_1 + \theta_2 + \frac{E_2}{\eta}}{F_S} \right) \cdot \tilde{P}_p(k) \\
& + \left[\left(\frac{\theta_1 + \theta_2 + \frac{E_2}{\eta}}{F_S} \right) - \frac{E_2(\theta_1 + \theta_2)}{\eta F_S^2} - 1 \right] \cdot \tilde{P}_p(k-1) + (E_1 + E_2) \\
& \cdot \tilde{P}_c(k + \Delta + 1) + \left[\left(\frac{\theta_1}{F_S} - 1 \right) (E_1 + E_2) + \frac{E_1 E_2}{\eta F_S} - E_1 - E_2 \right] \cdot \tilde{P}_c(k + \Delta) \\
& + \frac{\theta_2}{F_S} (E_1 + E_2) \cdot \tilde{P}_c(k - \Delta) + \left(\frac{\theta_1}{F_S} - 1 \right) \left(\frac{E_1 E_2}{\eta F_S} - E_1 - E_2 \right) \\
& \cdot \tilde{P}_c(k + \Delta - 1) + \frac{\theta_2}{F_S} \left(\frac{E_1 E_2}{\eta F_S} - E_1 - E_2 \right) \cdot \tilde{P}_c(k - \Delta - 1)
\end{aligned} \tag{2.10c}$$

where $\Delta = \tau F_S$, which was rounded to the nearest integer

The sampling frequency of 250 Hz was deemed to be sufficient for two reasons. Firstly, the sampling frequency was large enough to capture the major components of the circulatory waveforms, which consists of the heart rate and its harmonics (up to the 4th or 5th harmonics corresponding to roughly 5-6 Hz). Secondly, the errors in PTT estimation due to a resolution of 4 ms were roughly 11% for the carotid-brachial arterial path and 3% for the carotid-posterior-tibial arterial path.

2.3 Identifiability Analysis

The discretized models, (2.10a)-(2.10c), re-formulated as linear regression models in the form of $y = \phi^T \theta$, can be used to check for unique identifiability of model parameters [69]. The TLG model, (2.10a), re-written as

$$\tilde{P}_p(k+1) = [\tilde{P}_p(k) \quad \tilde{P}_c(k + \Delta + 1) \quad \tilde{P}_c(k + \Delta) \quad \tilde{P}_c(k - \Delta)] \begin{bmatrix} 1 - \frac{\theta_1 + \theta_2}{F_S} \\ E_1 \\ E_1 \left(\frac{\theta_1}{F_S} - 1 \right) \\ \frac{\theta_2 E_1}{F_S} \end{bmatrix}$$

shows that the system is overdetermined, but under ideal conditions (i.e. no noise) the parameters θ_1 , θ_2 , and E_1 can be uniquely identified. Similarly the parameters of the TLV model, (2.10b),

$$\tilde{P}_p(k+1)$$

$$= [\tilde{P}_p(k) \quad \tilde{P}_c(k+\Delta+2) \quad \tilde{P}_c(k+\Delta+1) \quad \tilde{P}_c(k+\Delta) \quad \tilde{P}_c(k-\Delta+1) \quad \tilde{P}_c(k-\Delta)] \begin{bmatrix} 1 - \frac{\theta_1 + \theta_2}{F_S} \\ \eta F_S \\ E_1 + \theta_1 \eta - 2\eta F_S \\ \frac{\theta_1 E_1}{F_S} - E_1 - \theta_1 \eta + \eta F_S \\ \theta_2 \eta \\ \frac{\theta_2 E_1}{F_S} - \theta_2 \eta \end{bmatrix}$$

and the TLS model, (2.10c),

$$\tilde{P}_p(k+1) = \begin{bmatrix} \tilde{P}_p(k) & \tilde{P}_p(k-1) & \tilde{P}_c(k+\Delta+1) & \tilde{P}_c(k+\Delta) & \dots \\ \dots & \tilde{P}_c(k-\Delta) & \tilde{P}_c(k+\Delta-1) & \tilde{P}_c(k-\Delta-1) \end{bmatrix} \begin{bmatrix} 2 - \frac{\theta_1 + \theta_2 + \frac{E_2}{\eta}}{F_S} \\ \left(\frac{\theta_1 + \theta_2 + \frac{E_2}{\eta}}{F_S} \right) - \frac{E_2(\theta_1 + \theta_2)}{\eta F_S^2} - 1 \\ E_1 + E_2 \\ \left(\frac{\theta_1}{F_S} - 1 \right) (E_1 + E_1) + \frac{E_1 E_2}{\eta F_S} - E_1 - E_2 \\ \frac{\theta_2}{F_S} (E_1 + E_2) \\ \left(\frac{\theta_1}{F_S} - 1 \right) \left(\frac{E_1 E_2}{\eta F_S} - E_1 - E_2 \right) \\ \frac{\theta_2}{F_S} \left(\frac{E_1 E_2}{\eta F_S} - E_1 - E_2 \right) \end{bmatrix}$$

are over-constrained but can be theoretically estimated uniquely.

2.4 Data Set

The data used in this thesis are electronically archived data from 133 human subjects that were originally obtained for a previous study under IRB approval and written informed consent [70]. All waveforms, archived as .mat files, were saved as ensemble averaged, single-beat waveforms, which were calibrated using mean and diastolic BP values calculated from brachial artery oscillometry. Oscillometry measures only SBP and DBP, but mean pressure can be calculated by

$$MP = \frac{SBP + 2DBP}{3} \quad (2.11)$$

Among the 133 subjects, 124 had brachial PVR waveforms and 99 had ankle PVR waveforms and all had carotid tonometry waveforms. It was important for the ankle PVR subjects to also have femoral tonometry recordings to be utilized in Chapter 3. Table 2.1 summarizes the characteristics of the subjects used in this investigation. Initially, more subjects were considered but some were excluded under one of 3 conditions with examples shown in Fig. 2.2.

1. Subjects with visibly corrupt recordings were excluded from the study.
2. In some subjects, the mean and/or diastolic BP discrepancy between carotid tonometry and peripheral PVR waveforms were significant due to imperfection of an automated process. These subjects were excluded as well.
3. In case of subjects with ankle PVR waveforms, femoral tonometry recording must be included and the PP associated with femoral tonometry must be greater than that associated with carotid tonometry following the principle of increasing PP with increasing distance from the heart [23], in addition to the mean and diastolic BP requirements listed above. Subjects with greater carotid tonometry PP than femoral tonometry PP were excluded.

Table 2.1: Model identification subject characteristics

Characteristics	n (number of subjects)	Median (IQR)
Male, %	133	67
Age Range	133	15-89
Carotid SBP (mmHg)	133	115.0 (103.7~132.4)
Carotid DBP (mmHg)	133	75 (64~86)
Carotid PP (mmHg)	133	41.6 (34.2~53.0)
Brachial Cuff SBP (mmHg)	124	111.6 (97.2~127.7)
Brachial Cuff DBP (mmHg)	124	75 (64~86)
Brachial Cuff PP (mmHg)	124	36.7 (30.5~44.6)
Ankle Cuff SBP (mmHg)	99	120.7 (107.7~136.1)
Ankle Cuff DBP (mmHg)	99	75 (65~86)
Ankle Cuff PP (mmHg)	99	46.2 (39.5~52.3)

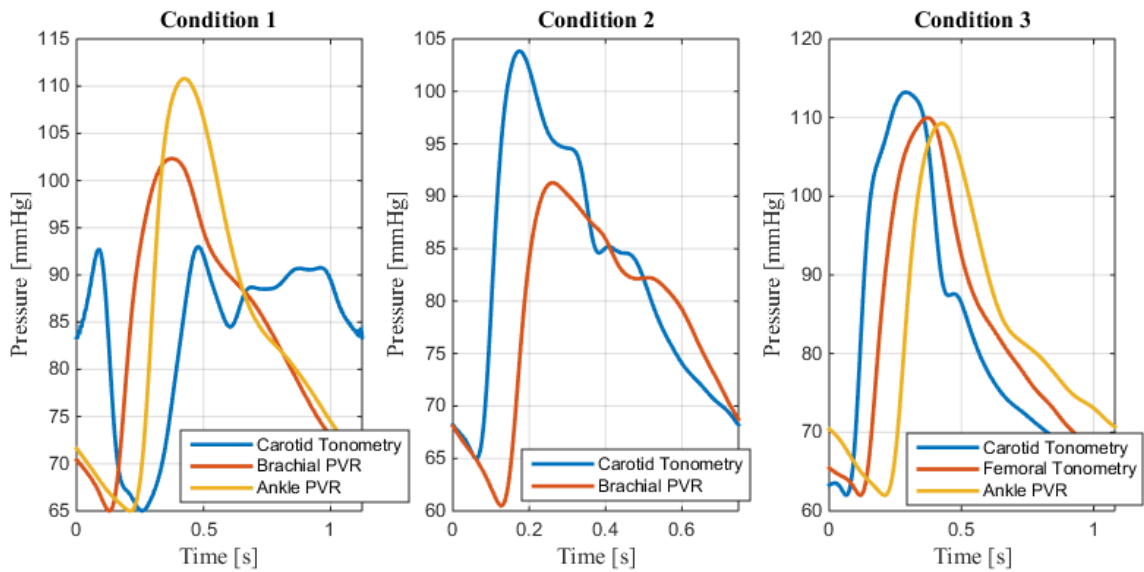


Fig. 2.2: Examples of conditions for exclusion of data. Incorrect morphology of carotid tonometry waveform (left), improper calibration (middle), and PP associated with femoral tonometry larger than that associated with carotid tonometry (right).

To prepare the data for model optimization, the single-beat waveforms were serially connected end-to-end in order to mimic physiologically stable conditions of more than 30 seconds.

2.5 Model Optimization via System Identification

The models were first computed by fitting them to the carotid tonometry waveform, $P_p(k)$, and corresponding distal PVR waveform. The reproduced carotid ABP waveform estimates, $\hat{P}_p(k, \Theta^*)$ were then compared with $P_p(k)$, where Θ^* is set of optimal parameters for each model that minimizes the following constrained optimization problem:

$$\Theta^* = \arg \min_{\Theta} \sqrt{\frac{1}{N} \sum_{k=1}^N [P_p(k) - \hat{P}_p(k, \Theta)]^2} \quad (2.12)$$

where the constraints were separately specified for each TLVE model. For the TLG model, $\Theta = \{\tau, \theta_1, \theta_2, E_1\}$ and the inequality constraints are:

$$\tau > 0, \quad 500 > \theta_1 > \theta_2 > 0.01, \quad E_1 > 0.0001$$

where all parameters must be positive because they represent physical components of the model. In particular $\theta_1 > \theta_2$ because $\theta_1 = \theta_2 + \frac{1}{R_T C_T}$ from (2.5). It follows that $\Theta = \{\tau, \theta_1, \theta_2, E_1, \eta\}$ and

$$\tau > 0, \quad 500 > \theta_1 > \theta_2 > 0.01, \quad E_1 > 0.0001, \quad \eta > 0.0001$$

are the parameters and constraints for the TLV model, and lastly $\Theta = \{\tau, \theta_1, \theta_2, E_1, \eta, E_2\}$ and

$$\tau > 0, \quad 500 > \theta_1 > \theta_2 > 0.01, \quad E_1 > 0.0001, \quad \eta > 0.0001, \quad E_2 > 0.0001$$

are the parameters and constraints for the TLS model. For all three models, the upper and lower boundaries for τ were set according to anatomically realistic values. For the

carotid-brachial artery path, the boundaries were 0.11 s and 0.004 s while the boundaries for the carotid-posterior-tibial artery path were 0.18 s and 0.08 s.

2.6 Results

2.6.1 Estimation of Carotid Arterial Blood Pressure

Fig. 2.3 shows examples of measured and optimized carotid ABP waveforms at (a) the upper arm and (b) the ankle. Among the three models for (a) it is clear that TLS model provides the most accurate waveform, but it is not the case for the ankle in (b). In fact, no model stands out as the best suited for describing the relationship between carotid artery tonometry and ankle PVR.

These findings are further supported by Table 2.2 which lists the shape and central ABP errors root-mean-squared across all subjects. The root-mean-square was applied as opposed to mean \pm standard deviation or median (IQR) in order to compensate for a non-Gaussian distribution of results and to present accuracy and precision of the model for each metric (e.g. SBP error and PP error) into a single value. To evaluate statistical significance between models a paired t-test was used with $p < 0.0167$ as significant based on the Bonferroni correction to counteract multiple comparisons.

Compared to the TLG model, TLV and TLG were superior in for both upper arm and ankle. In the upper arm especially, TLS greatly outperformed TLG and TLV. Even though TLV reduced all error metrics except for PP error, the differences were marginal compared to the improvements provided by TLS. For the ankle, surprisingly, TLV performed better than TLS with smaller RMSE and SP error. Realistically, all three models performed similarly for the ankle and TLG and TLV performed similarly for the upper arm.

The distribution of error and the relative performance of three physical models can be easily visualized by Bland-Altman plots in Fig. 2.4. In the upper arm, the differences of the mean and distribution of error between TLG and TLV were minimal while TLS displayed very narrow limits of agreement. In estimating central ABP from ankle PVR, there were only minimal differences between TLG, TLV, and TLS as supported by Fig. 2.3(b) and Table 2.2.

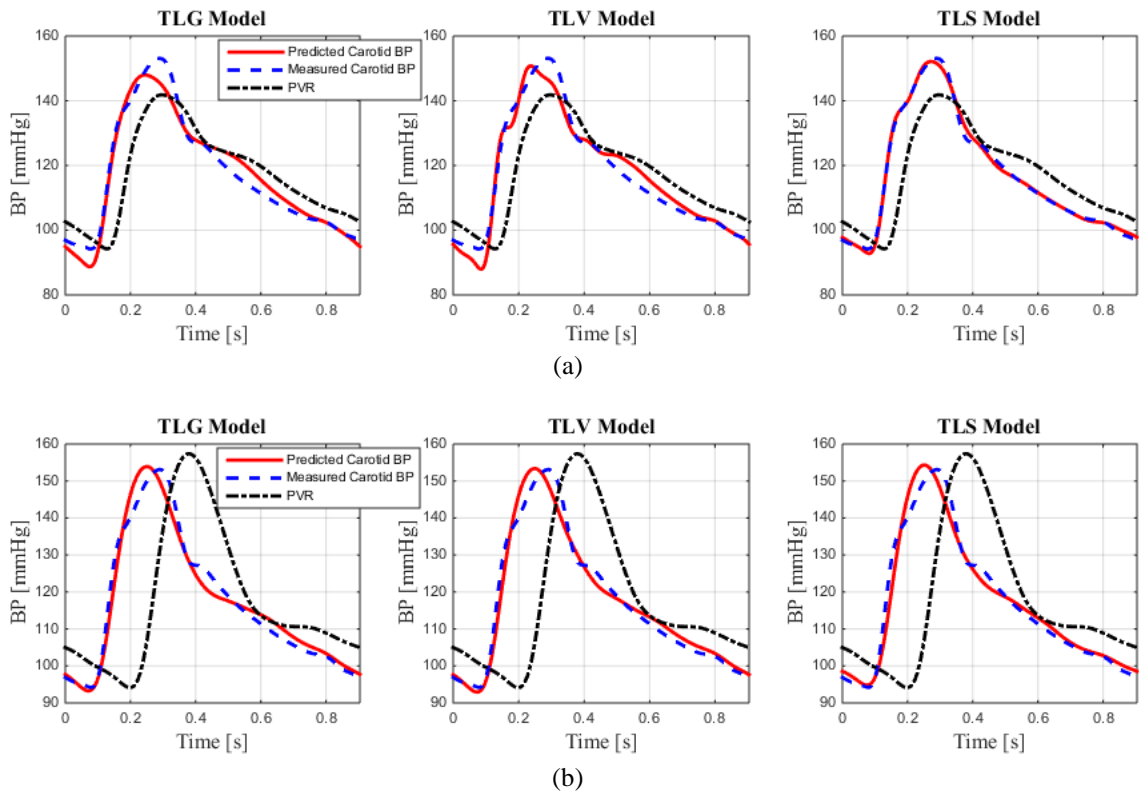


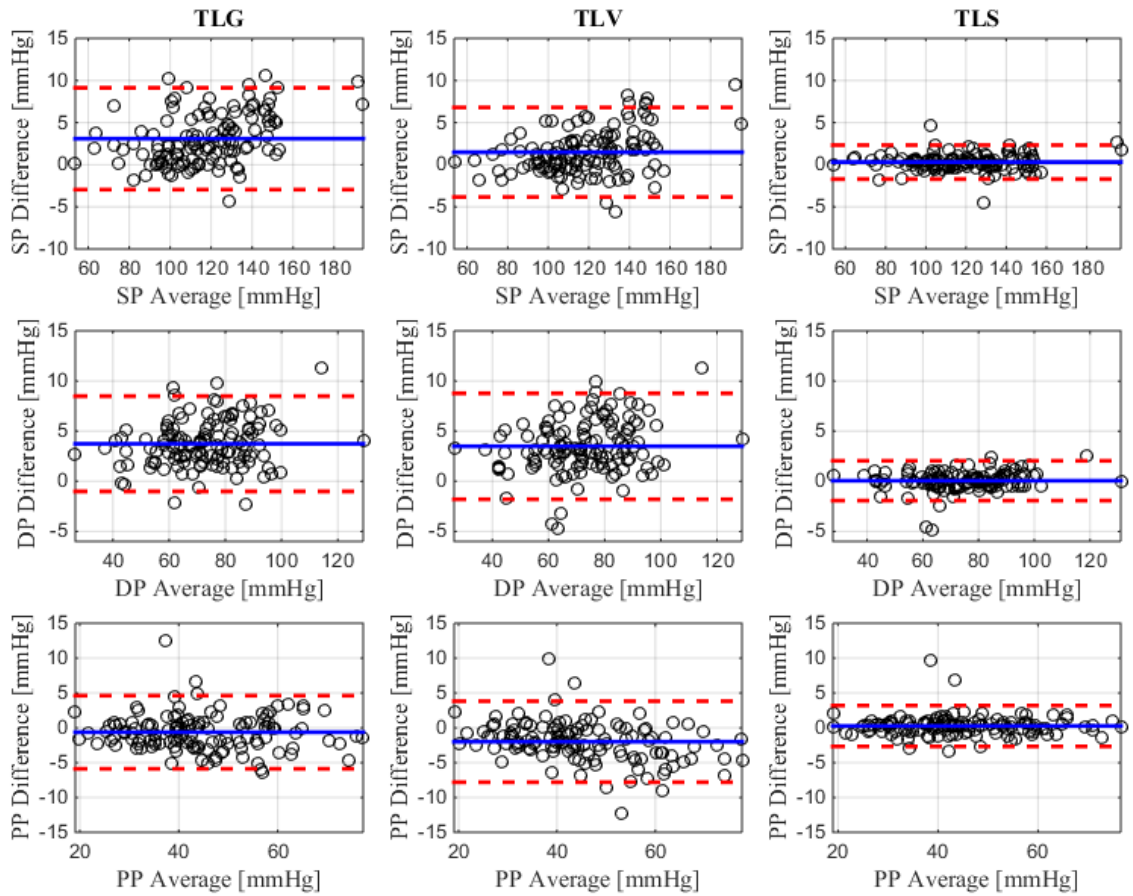
Fig. 2.3: Representative example of measured ($P_p(k)$) and model-predicted ($\hat{P}_p(k, \theta^*)$) carotid artery tonometry waveform as well as measured pulse volume waveform (PVR) ($P_C(k)$). (a) Upper arm. (b) Ankle.

Table 2.2: TLVE error results

	Upper Arm			Ankle		
	TLG	TLV	TLS	TLG	TLV	TLS
RMSE [mmHg]	3.2	2.8 [†]	1.2 ^{††}	2.9	2.5 [†]	2.6 ^{††}
SBP Error [mmHg]	4.3	3.0 [†]	1.1 ^{††}	2.1	2.1	2.2
DBP Error [mmHg]	4.6	4.5	1.0 ^{††}	1.7	1.5	1.3 [†]
PP Error [mmHg]	2.7	3.5	1.5 ^{††}	2.3	2.2	2.2

RMSE: root-mean-squared error between carotid tonometry and estimated carotid ABP waveform.

[†]: p<0.0167 compared with TLG. ^{††}: p<0.0167 compared with TLV.



(a)

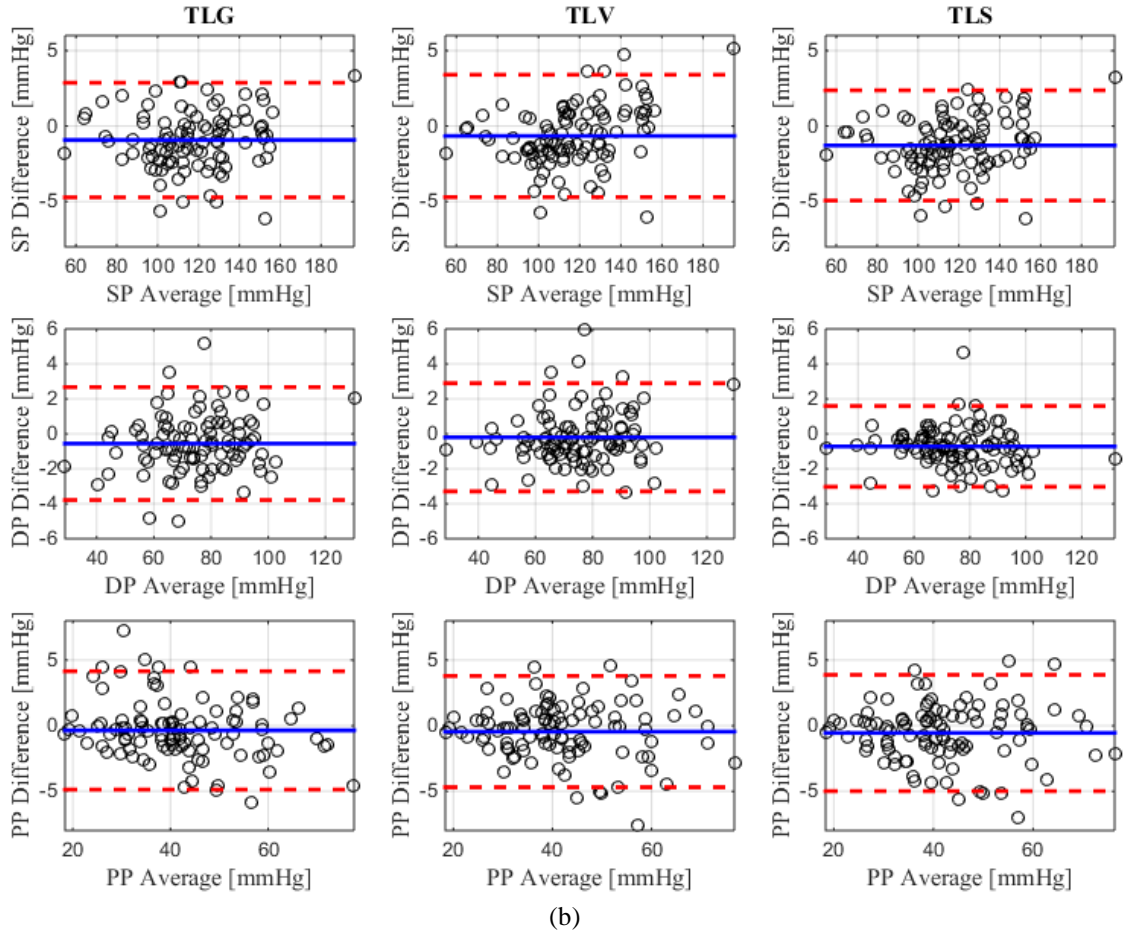


Fig. 2.4: Bland-Altman plots associated with carotid SP, DP, and PP in all subjects derived from (a) upper arm PVR and (b) ankle PVR.

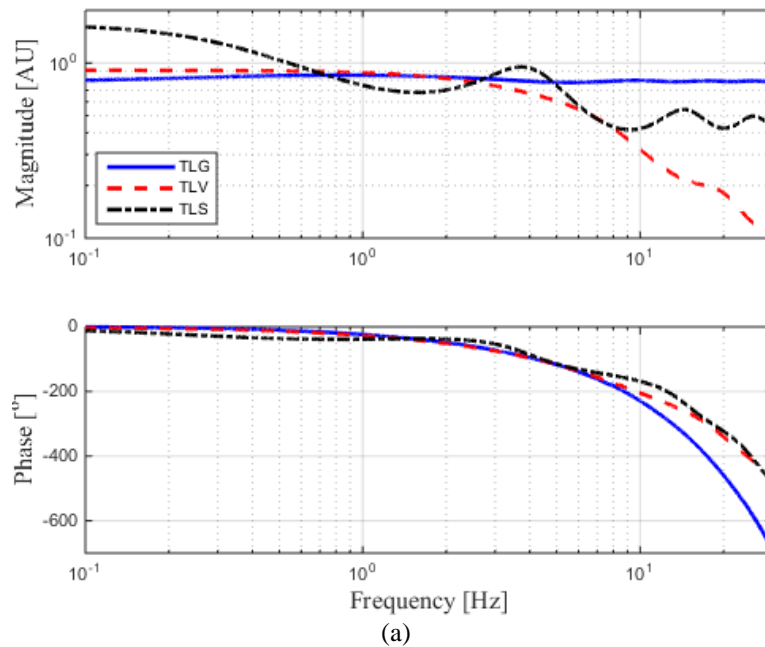
2.6.2 Frequency Response Results

For the carotid-brachial arterial path, the frequency responses of TLG and TLV were very close to each other up to 3 Hz (Fig. 2.5(a)). At greater than 3 Hz, TLG maintains a relatively flat magnitude response while TLV exhibits behaviors established for single-pole filters, similar to the Voigt model. The frequency response associated with TLS in the upper arm was largely different from those of TLV and TLG, especially the DC gain (TLV: 0.9; TLS: 1.7). Additionally, the pole locations were not close to each other (TLV: 3.7 Hz; TLS: 0.4 Hz), and the zero location of the TLS model was very

small (1.4 Hz). The TLV model, which is equipped with only one pole, cannot replicate the frequency response of the TLS model.

For the carotid-posterior-tibial arterial path the frequency response associated with TLG was slightly different compared to those of TLV and TLS and not the degree of TLG in the upper arm. The frequency responses of TLV and TLS were nearly identical for the ankle up to very high frequency regions (~30 Hz) which is outside of the frequency regime associated with the energy content in arterial waveforms. The DC gains were very similar (TLV: 1.0; TLS: 1.1) as were the pole locations (TLV: 6.6 Hz; TLS: 3.6 Hz). Finally, the zero location associated with the TLS model was very far from the pole locations (14.6 Hz), minimizing its influence on the BP waveforms.

Table 2.3 continues the trend of significantly different results between TLVE models for the carotid-brachial arterial path (Table 2.3(a)) while the results for the carotid-posterior-tibial arterial path are very similar (Table 2.3(b)).



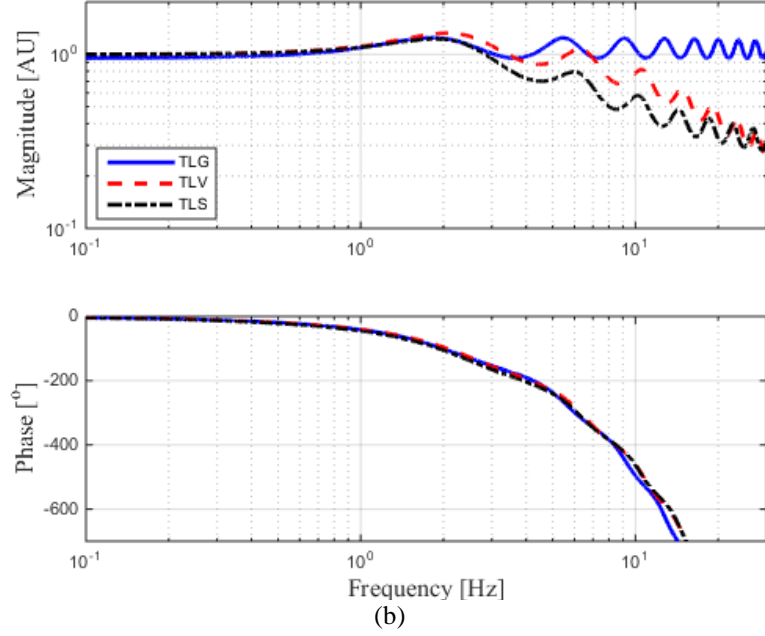


Fig. 2.5: Frequency responses associated with TLG, TLV, and TLS models. (a) Upper arm. (b) Ankle.

Table 2.3: Optimal model parameters associated with TLG, TLV, and TLS models (Median (IQR))

	τ [ms]	θ_1 [s ⁻¹]	θ_2 [s ⁻¹]	E_1 [au]	η [s]	E_2 [au]
TLG	64 (60~76)	0.8 (0.4~31.4)	0.6 (0.2~5.1)	1.3 (1.2~1.4)	N/A	N/A
TLV	36 (24~52) [†]	210 (24~437) [†]	19 (3~57) [†]	1.1 (1.0~1.2) [†]	0.05 (0.02~0.08)	N/A
TLS	44 (40~52) ^{†‡}	22 (13~32) ^{†‡}	12 (7~18) [‡]	0.6 (0.2~0.7) ^{†‡}	0.2 (0.1~0.3) [‡]	1.6 (1.2~1.8)

(a)

	τ [ms]	θ_1 [s ⁻¹]	θ_2 [s ⁻¹]	E_1 [au]	η [s]	E_2 [au]
TLG	140 (120~160)	390 (31~434)	52 (4~92)	1.1 (1.0~1.1)	N/A	N/A
TLV	120 (100~130) [†]	390 (247~443)	60 (10~109)	1.0 (0.95~1.1) [†]	0.02 (0.01~0.04)	N/A
TLS	120 (110~140) ^{†‡}	388 (346~442)	58 (15~109)	0.9 (0.7~1.0) ^{†‡}	0.03 (0.01~0.36) [‡]	2.9 (1.2~11.9)

(b)

[†]: $p < 0.0167$ compared to TLG. [‡]: $p < 0.0167$ compared to TLV.

2.6.3 Akaike Information Criterion

Akaike Information Criterion (AIC) is a metric to evaluate the accuracy-complexity tradeoff for each mode. For each subject, an AIC value was assigned to each model. Then the number of subjects for which a model had the smallest AIC value, a measure of best accuracy-complexity tradeoff, was counted. AIC indicated that TLS and TLV models were the best options for the upper arm and ankle, respectively (Table 2.4).

Table 2.4: Akaike information criterion

	TLG	TLV	TLS
Upper Arm	0	5	119
Ankle	3	78	18

2.7 Discussion

Due to the simple measuring procedure along with morphological similarity to ABP waveforms, PVR is an attractive non-invasive surrogate of ABP waveform. Yet the waveforms are inherently volume recordings, not pressure, and they often lack the complex morphology of ABP waveforms. The goal of this study was to develop models for the carotid-brachial and carotid-posterior-tibial arterial paths in order to overcome the flaws and further improve its appeal as a staple in routine CV health monitoring.

2.7.1 Relationship between Central Aortic BP and Distal PVR

The results overwhelmingly favor the TLS model for the upper arm but are inconclusive for the ankle. The results indicate that viscoelasticity is not as important at the ankle and that the difference between ankle ABP and ankle PVR may be minimal. In

fact, disregarding shape error (RMSE in Table 2.2), TLG may be the best model due to its simplicity and comparable accuracy in estimating central ABP from A PVR.

For the upper arm, the results suggest viscoelasticity played a more central role in a large percentage of subjects in which the brachial PVR pulse amplitude was smaller than the carotid tonometry pulse pressure. Despite being equipped with parameters to predict pulse pressure amplification, it was rarely observed in TLG and TLV results. In fact, the frequency response and optimized parameter values in Table 2.3 show that TLG and TLV exhibited a relatively flat frequency response. For the TLG model, the TL component of the model reduced to $e^{-\tau s}$, since θ_1 and θ_2 were very small. Similarly, the TL component of the TLV model reduced to $e^{-\tau s}$ since θ_1 was much larger than θ_2 . The less complex TLG and TLV models struggled in comparison while TLS was highly effective. The different conclusions for the separate pathways suggest that the oscillometric cuff is not a major cause of distortions in the wave. Had the cuff mechanics played a bigger part in distorting ankle ABP, the results for the carotid-ankle pathway may have been more like those for the carotid-brachial pathway. Yet it is undeniable that the carotid-brachial arterial path was better modeled when viscoelasticity was heavily considered. It is plausible that the tissues coupling the arterial vessel to BP cuff play a non-negligible role in this relationship as more tissue typically surrounds the brachial artery at the upper arm than the posterior-tibial artery at the ankle.

2.7.2 Limitations

There were two main limitations of this study that may need to be addressed in the future. Carotid artery tonometry is a noninvasive gold standard method of recording BP waveforms but for investigative purposes, invasive aortic BP would be ideal. Second,

this investigation was not an exhaustive review of established viscoelastic models. Therefore it can only be concluded that among the three physical models examined, TLS is better suited for the carotid-brachial arterial path while TLV or TLG may be sufficient for the carotid-posterior-tibial arterial path.

Chapter 3: Wave Reflection Quantification Using Estimated Central and Peripheral Blood Pressure Waveforms

In Chapter 2, models were selected to represent the relationship between carotid tonometry and distal PVR. This chapter will employ the TLV model to estimate central ankle ABP from ankle PVR and use it along with carotid tonometry to calculate forward and backward BP waves via a technique previously shown to be effective on swine [71].

3.1 Problem Formulation

The arterial tree can be modeled as a lossless tube, such as the TL model utilized in Chapter 2, meaning that forward and backward BP waves propagate along the tube without experiencing changes in morphology. The BP waves at the inlet, $P_P(k)$, and the outlet, $P_D(k)$, can be formulated as the sum of forward and backward BP waves properly shifted for the corresponding location.

$$\begin{aligned} P_P(k) &= P_f(k + \Delta) + P_b(k - \Delta) \\ P_D(k) &= P_f(k) + P_b(k) \end{aligned} \quad (3.1)$$

where $\Delta = \tau F_S$ and τ and F_S are PTT and sampling frequency, respectively. Assuming the subject is in a stable physiological state, the follow relationships hold true:

$$\begin{aligned} P_f(k + \Delta) &= P_f(k + \Delta - N) \text{ if } k + \Delta > N \\ P_b(k - \Delta) &= P_b(k - \Delta + N) \text{ if } k - \Delta < 0 \end{aligned} \quad (3.2)$$

where N is the number of data samples in a single heartbeat. As a result, (2.13) results in $2N$ equations, 2 for each $k = 1 \cdots N$. Substituting the relationship in (3.2) when required, (2.13) can be stacked to build the following matrix equation:

$$A_{2N \times 2N} X_{2N \times 1} = B_{2N \times 1} \quad (3.3)$$

where

$$X_{2N \times 1} = [P_f(1) \cdots P_f(N) P_b(1) \cdots P_b(N)]^T \quad (3.4)$$

$$B_{2N \times 1} = [P_D(1) \cdots P_D(N) P_P(1) \cdots P_P(N)]^T \quad (3.5)$$

$$A_{2N \times 2N} = \begin{bmatrix} A_1 \\ A_2 \end{bmatrix} = \begin{bmatrix} I_{\Delta \times \Delta} & 0_{\Delta \times (N-\Delta)} & I_{\Delta \times \Delta} & 0_{\Delta \times (N-\Delta)} \\ 0_{(N-\Delta) \times \Delta} & 0_{\Delta \times (N-\Delta)} & 0_{(N-\Delta) \times \Delta} & I_{(N-\Delta) \times (N-\Delta)} \\ 0_{(N-\Delta) \times \Delta} & I_{(N-\Delta) \times (N-\Delta)} & 0_{\Delta \times (N-\Delta)} & I_{\Delta \times \Delta} \\ I_{\Delta \times \Delta} & 0_{\Delta \times (N-\Delta)} & I_{(N-\Delta) \times (N-\Delta)} & 0_{(N-\Delta) \times \Delta} \end{bmatrix} \quad (3.6)$$

It can be easily seen from (3.6) that the rows of A is linearly dependent but it is addressed by imposing stacking additional physiologically relevant equations. Specifically, central aortic flow is zero during diastole and this characteristic can be formulated as

$$Q_0(k) = \frac{P_f(k + \Delta) - P_b(k - \Delta)}{Z_c} = 0 \quad (3.7)$$

where $Q_0(k)$, $\delta N < k \leq N$ corresponds to aortic flow during diastole. Incorporating (3.7) into (3.3) over constrains the once ill-conditioned matrix equation.

$$A_{(3-\delta)N \times 2N} X_{2N \times 1} = B_{(3-\delta)N \times 1} \quad (3.8)$$

(3.8) can be solved by the least-squares method by pre-multiplying the pseudo-inverse of $A_{(3-\delta)N \times N}$ to both sides of (3.8), or

$$X = [A^T A]^{-1} A^T B \quad (3.9)$$

As described in (3.4), once X is determined it can be separated into $P_f(k) = X(1:N)$ and $P_b(k) = X(N + 1:2N)$.

3.2 Data Set

For the study, the same 99 subjects with carotid tonometry and ankle PVR data were used. Recall that this data set also included femoral tonometry recordings as well. Since carotid tonometry and femoral tonometry are established, high-fidelity BP measurement modalities, the wave reflection calculated from carotid tonometry and femoral tonometry waveforms was used as the reference method to evaluate the wave reflection calculated from carotid tonometry and estimated ankle ABP waveforms. This

method allows for direct evaluation of estimated ankle ABP waveforms as a potential surrogate of femoral tonometry.

Table 3.1: Wave reflection subject characteristics

Characteristics	Median (IQR)
Male, %	43
Age Range	15-81
Carotid SBP (mmHg)	113.8 (100.7~130.5)
Carotid DBP (mmHg)	75 (65~86)
Carotid PP (mmHg)	40.2 (33.2~48.6)
Ankle Cuff SBP (mmHg)	120.7 (107.7~136.1)
Ankle Cuff DBP (mmHg)	75 (65~86)
Ankle Cuff PP (mmHg)	46.2 (39.5~52.3)
Femoral SBP (mmHg)	120.9 (107.4~133.8)
Femoral DBP (mmHg)	75 (65~86)
Femoral PP (mmHg)	45.5 (38.9~54.4)

3.3 Methods

First, ankle ABP waveform was estimated by applying ankle PVR to the Voigt model component of the individualized TLV model. Then PTT between carotid tonometry and ankle ABP waveform was estimated by the time delay between the two waveforms. The tunable constraint parameter, δ , offers some freedom. The relative duration of diastole is roughly 30% of the cardiac cycle. Setting $\delta = 0.5$, which was used in a previous study to sufficiently constrain the problem [71], forward and backward BP waves were calculated using (3.9).

This technique, while novel and physics based, is limited by the $2N$ degrees of freedom. The minor flaw is manifested in the form of non-differentiable forward and

backward waves as shown in Fig. 3.1(a). It can be remedied by applying a low-pass filter ($\omega_c = 5$ Hz in this study) but information may be lost in the process and is not ideal. From the filtered forward and backward BP waves, the corresponding pulse pressures, $|P_f|$ and $|P_b|$ can be extracted and used to calculate reflection magnitude ($RM = \frac{|P_b|}{|P_f|}$) and reflection index ($RI = \frac{|P_b|}{|P_f| + |P_f|}$).

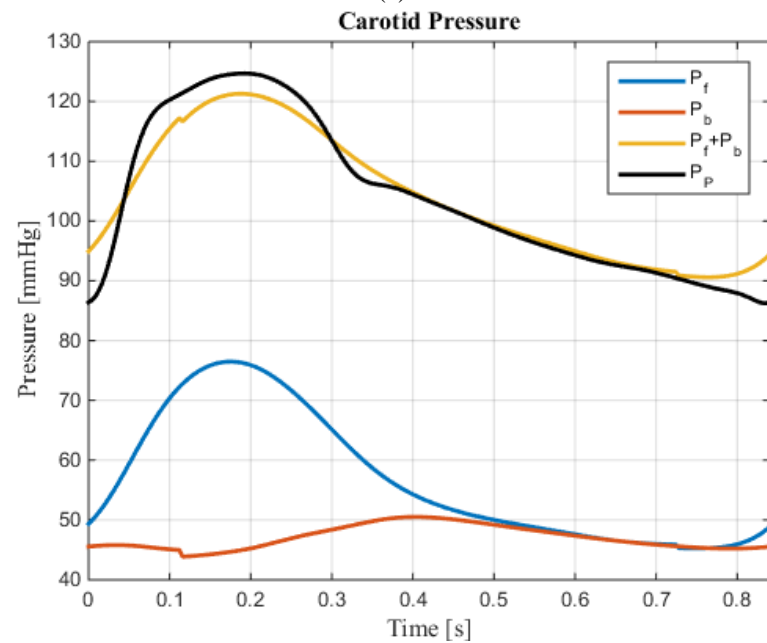
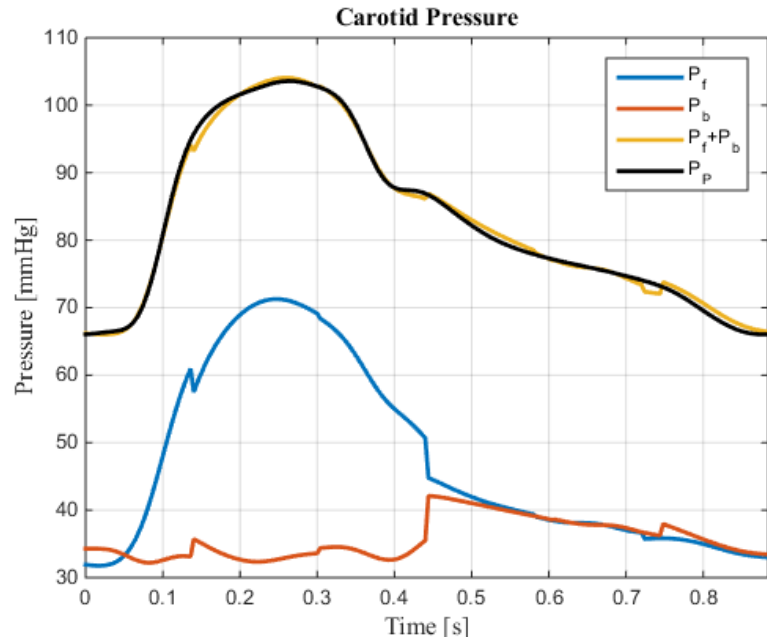
3.4 Results

As mentioned above, the process of filtering degraded the goodness of fit between the sum of shifted forward and backward BP waves and (b) carotid tonometry and (c) estimated ankle ABP waveform. However, the end results were promising. The decomposed waves, P_f and P_b were shifted to estimate the femoral ABP waveform. Since the BP pulse travels from the heart and through the femoral artery (near groin area) to reach the ankle, it is not unreasonable to expect estimated femoral pressure to be similar in shape to femoral tonometry in ideal conditions. Simultaneously, forward and backward BP waves decomposed from carotid tonometry and femoral tonometry, $P_{f,ref}$ and $P_{b,ref}$ were compared P_f and P_b (Fig. 3.1(d)).

The average estimations of $|P_f(t)|$, $|P_b(t)|$, RM and RI were close in magnitude to those from the reference method (Table 3.2), however Fig. 3.2 and Table 3.3 indicate that there is much room for improvement. Estimated carotid-ankle PTT correlated acceptably with carotid-femoral PTT, but the correlations of estimated and reference RM and RI were marginally acceptable. Fig. 3.2(a) shows that there is a slight trend between estimated and reference RM and RI but also that there is non-trivial spread, decreasing the correlation. Additionally, the Bland-Altman plots (Fig. 3.2(b)) suggest that this

method underestimates larger RM and RI while overestimating smaller RM and RI when compared with the reference method.

$|P_f(t)|$ and $|P_b(t)|$ were highly correlated with $|P_{f,ref}(t)|$ and $|P_{b,ref}(t)|$ but individual PPs contain little information on the health or potential risk since wave reflection quantified as the ratio of forward and backward pulse pressures.



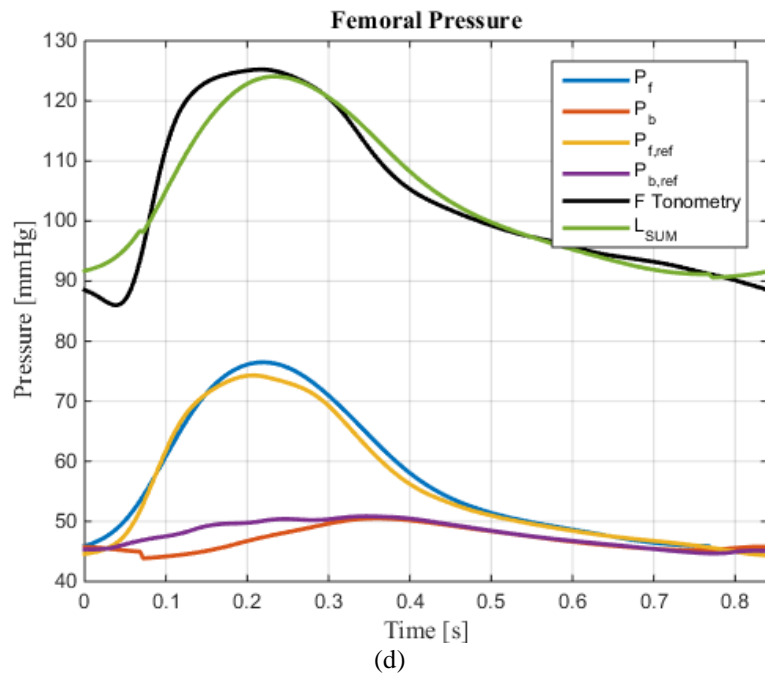
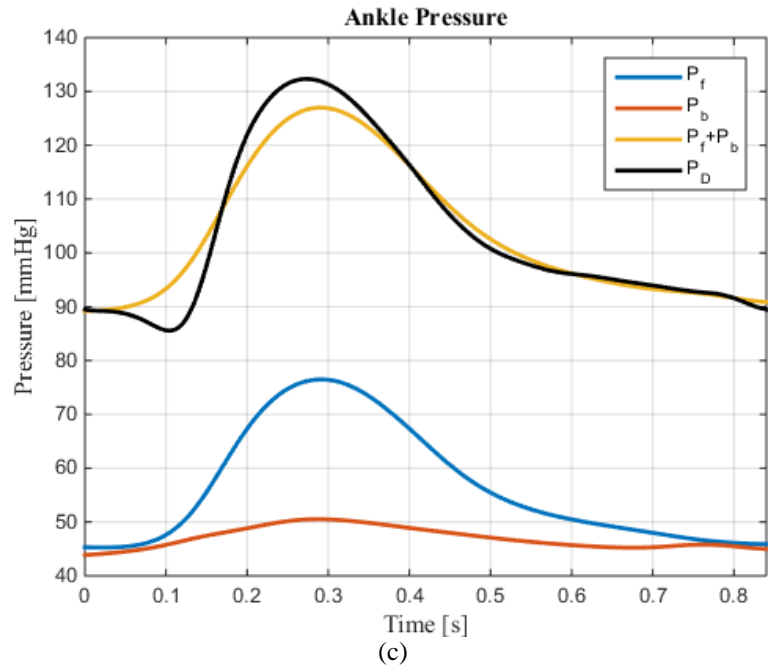


Fig. 3.1: An example of wave decomposition, with reconstruction of ABP waveforms at (a) carotid artery using unfiltered forward and backward BP waves (b) carotid artery, (c) posterior-tibial artery, and (d) femoral artery.

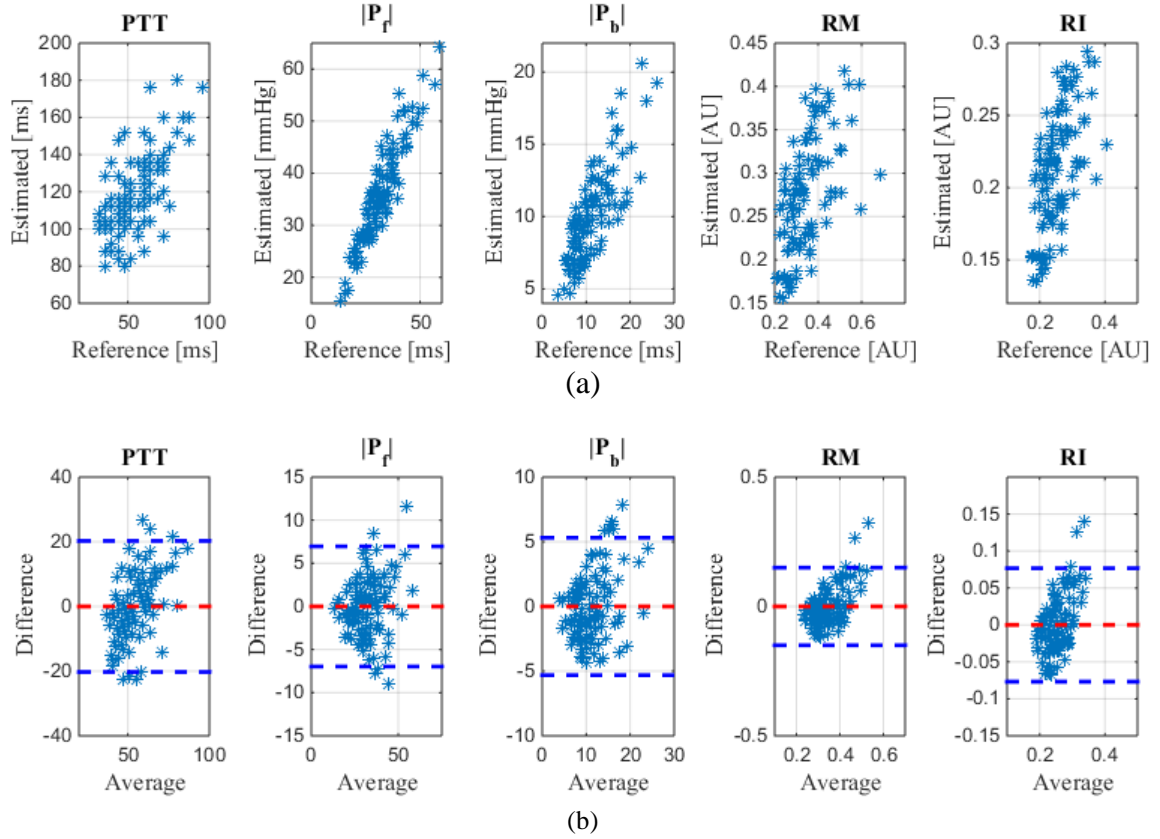


Fig. 3.2: Correlation and Bland-Altman plots associated with PTT, $|P_f(t)|$, $|P_b(t)|$, RM and RI. (a) Correlation plots. (b) Bland-Altman plots.

Table 3.2: Reference and estimated CV risk predictors

n=64	PTT [ms]	$ P_f(t) $ [mmHg]	$ P_b(t) $ [mmHg]	RM [AU]	RI [AU]
Reference	56 ± 14	32 ± 10	12 ± 5	0.37 ± 0.11	0.27 ± 0.16
Estimated	119 ± 22	37 ± 10	10 ± 4	0.28 ± 0.07	0.22 ± 0.04

Table 3.3: Correlations between reference and cstimated CV risk predictors

n=64	PTT	$ P_f(t) $	$ P_b(t) $	RM	RI
R	0.68	0.93	0.83	0.53	0.54

3.5 Discussion

The lack of a clear metric to optimize the performance proved to be challenging. Unlike the models developed in Chapter 2, which were optimized via an explicit objective function to minimize the error between estimated and measured central ABP waveforms, this technique more heavily dependent on the data, which are not perfect. Specifically, estimated ankle ABP waveform was used with the assumption that the TLV model adequately captured the lumped dynamics of the arterial vessel, tissue, and BP cuff, however there may be better suited models that would produce more powerful results.

In addition to the imperfections associated with the data, the tunable parameter δ opens possibilities for refining the problem. Since δ is directly connected to the least-squares-solution, (3.9), a potential algorithm to identify an optimal δ specific to each subject is appealing. For example, as δ changes the resulting forward and backward BP waves will change in morphology as well. Exploiting the common occurrence of non-differentiable, step-wise-like forward and backward BP waves (Fig. 3.1(a)) an algorithm to identify δ at which the forward and backward waves are free of such discontinuities may benefit the solution. A few adaptations of δ optimizing algorithms were tested but they were unsuccessful in outperforming the technique with $\delta = 0.5$. In an attempt to bypass the issue surrounding δ , matrix regularization was applied to avoid an ill-conditioned matrix equation with little success.

Wave reflection quantification offers valuable insight regarding the CV health, specifically the arterial tree, when used with highly accurate waveforms such as invasive measurements [2], [7], [21], [61]–[66]. Although not yet robust against ABP

measurement or estimation errors, the matrix equation based method studied in this chapter has much potential for being incorporated into routine practice.

Chapter 4: Two-Sensor Blind System Identification

4.1 Introduction to Individualized Transfer Functions

ITF offers an inherent advantage over GTF due to its ability to select model parameters unique to each case. In the case of modeling the cardiovascular system via a TL model, an individualized, subject-specific model is able to identify pulse transit time, τ , and tube-load parameters, θ_1 and θ_2 , that are different for each subject. Additionally, GTF was shown to be less able to compensate for higher frequency components present in the ABP waveform, which typically carry individualized information, while ITF was able to extract relevant information [72].

As a result, methodologies involving ITF have been increasingly reported, as shown in Table 1.1. Specifically, studies have shown that central ABP can be estimated via two-channel blind system identification (i.e. having no input information) by applying an ITF to two invasive peripheral BP measurements (e.g. femoral and radial ABPs) in swine [50] and in humans [55]. The model consisted to two asymmetric TL models connected in parallel branched from a common source, similar to the anatomy of the human arterial tree shown in Fig. 4.1. This chapter presents and evaluates a similar model applied to brachial and ankle PVR measurements in order to avoid the need for specialized tonometry or even invasive measurements.

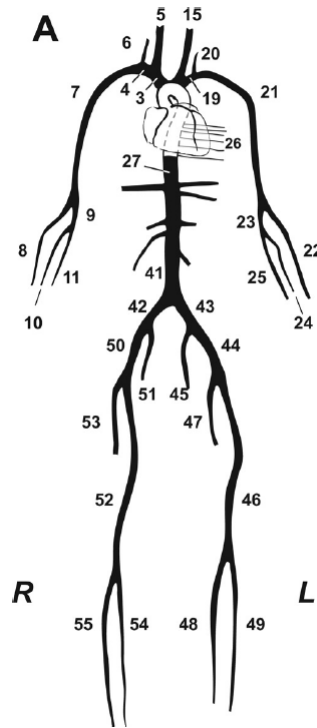


Fig. 4.1: Schematic of human arterial tree from Reymond, *et al.* [73]. 21: Brachial Artery; 44: Femoral Artery

4.2 Model of Human Arterial Tree

It was concluded in Chapter 2 that the TLS model best relates brachial PVR waveform to carotid tonometry. For the carotid-ankle PVR relationship, the three models studied showed minimal differences in accuracy. Further, the median value for the gain, E_1 , in the TLG model was very close to 1 (Table 2.3). In order to reduce the number of parameters, decreasing both complexity of the model and variance of the included parameters, E_1 was treated as a constant with a value of 1. Therefore, TLS and simple TL models were employed for the two-channel cuff model shown in Fig. 4.2.

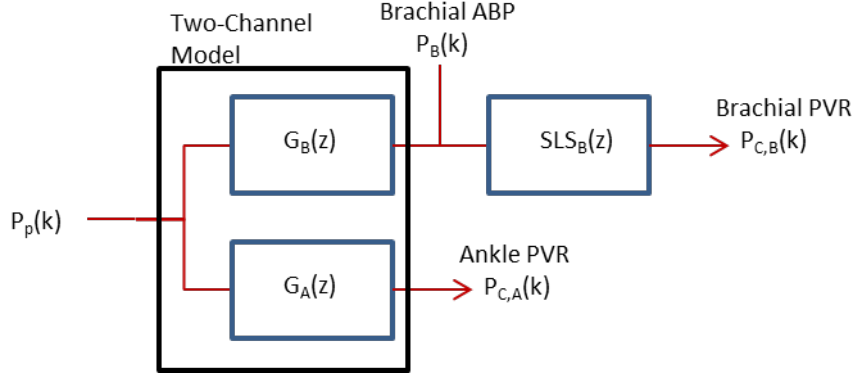


Fig. 4.2: Two-sensor cuff model. $G_B(z)$: TL model associated with carotid-brachial arterial path; $G_A(z)$: TL model associated with carotid-posterior-tibial arterial path

4.3 Mathematical Formulation of Blind System Identification Problem

Exploiting the common input, $P_p(k)$, of the two parallel channels, it can be shown that

$$\hat{P}_{P,B}(s) = G_B^{-1}(s)SLS_B^{-1}(s)P_{C,B}(s) = P_P(s) = G_A^{-1}(s)P_{C,A}(s) = \hat{P}_{P,A}(s) \quad (4.1)$$

$$\begin{aligned} & \frac{(s + \theta_{1B})e^{\tau_B s} + \theta_{2B}e^{-\tau_B s}}{s + \theta_{1B} + \theta_{2B}} \cdot \frac{E_{1B}E_{2B} + (E_{1B} + E_{2B})\eta_B s}{E_{2B} + \eta_B s} P_{C,B}(s) \\ &= \frac{(s + \theta_{1A})e^{\tau_A s} + \theta_{2A}e^{-\tau_A s}}{s + \theta_{1A} + \theta_{2A}} P_{C,A}(s) \end{aligned} \quad (4.2)$$

where $\hat{P}_{P,B}$ is the central ABP estimated from brachial PVR and $\hat{P}_{P,A}$ is the central ABP estimated from ankle PVR. Equation (4.2) cannot be explicitly satisfied, but P_P can be estimated in two steps by first identifying the SLS model, then the two-sensor ITF.

Using the forward difference approximation, $s \approx F_S(z - 1)$, the SLS model can be re-written as

$$\begin{aligned} P_P(k+1) &= \left(1 - \frac{E_{2B}}{\eta_B F_S}\right) P_P(k) + (E_{1B} + E_{2B})P_C(k+1) \\ &\quad + \left(\frac{E_{1B}E_{2B}}{\eta_B F_S} - E_{1B} - E_{2B}\right) P_C(k) \end{aligned} \quad (4.3)$$

as well as the TL models associated with the two-channel model.

$$\begin{aligned} \hat{P}_{P,B}(k+1) &= \left(1 - \frac{\theta_{1B} + \theta_{2B}}{F_S}\right) \cdot \hat{P}_{P,B}(k) + P_C(k + \Delta_B + 1) + \left(\frac{\theta_{1B}}{F_S} - 1\right) \cdot P_C(k + \Delta_B) + \frac{\theta_{2B}}{F_S} \\ &\quad \cdot P_C(k - \Delta_B) \end{aligned} \quad (4.4)$$

$$\begin{aligned} \hat{P}_{P,A}(k+1) = & \left(1 - \frac{\theta_{1A} + \theta_{2A}}{F_S}\right) \cdot \hat{P}_{P,A}(k) + P_C(k + \Delta_B + \delta_\Delta + 1) + \left(\frac{\theta_{1A}}{F_S} - 1\right) \\ & \cdot P_C(k + \Delta_B + \delta_\Delta) + \frac{\theta_{2A}}{F_S} \cdot P_C(k - \Delta_B - \delta_\Delta) \end{aligned} \quad (4.5)$$

where $\delta_\Delta = \Delta_A - \Delta_B = (\tau_A - \tau_B)F_S > 0$ is the sample difference between ankle PVR and estimated brachial ABP waveform, assuming τ_A is larger than τ_B . If it is not the case, then (4.4) and (4.5) are adjusted accordingly so that $\Delta_B = \Delta_A + \delta_\Delta$, where $\delta_\Delta = (\tau_B - \tau_A)F_S$. Since brachial ABP waveform, \hat{P}_B , is first estimated, the PTT between \hat{P}_B and $P_{C,A}$ is used to δ_Δ .

4.4 Identifiability Analysis

Unlike the TLVE models discussed in Chapter 2, the lumped two-sensor cuff model was not identifiable in a single optimization. Therefore the model was separated into a two-channel model and SLS model.

The two-channel model was previously shown to be identifiable under most physiological conditions [55]. In summary the load characteristics associated with the two channels representing the arterial branches of upper and lower body extremities are highly different. In the extreme case that they are very similar, the problem re-forms into a single-channel problem ($P_{C,B} = P_{C,A}$) and cannot be uniquely identified without input information. Another condition of identifiability, known as the ‘‘blind identifiability condition,’’ states that the PTT to each of the measurement locations and the sampling frequency must be large enough. That is,

$$\Delta_B = \tau_B F_S \geq 1, \quad \Delta_A = \tau_A F_S \geq 1 \quad (4.6)$$

Equation (4.6) can be easily satisfied with proper selection of BP measurement locations and sampling frequency.

The identifiability of the SLS model can be address by analyzing the discretized equation, (4.3), similar to what was done in Chapter 2. First, $\frac{E_{2B}}{\eta_B}$ and $E_{1B} + E_{2B}$ can be uniquely identified by the regressors $P_p(k)$ and $P_c(k + 1)$ respectively. Then E_{1B} can be calculated by identifying the coefficient $\left(\frac{E_{1B}E_{2B}}{\eta_B F_S} - E_{1B} - E_{2B}\right)$ and using the values obtained for $\frac{E_{2B}}{\eta_B}$ and $E_{1B} + E_{2B}$. Finally E_{2B} and η_B can be realized from the previous relationships.

4.5 Model Optimization

Identifying the SLS model requires knowledge of the input to the system, the brachial ABP. While this information was not directly available, the process of calibrating the measured waveforms offered insight regarding the brachial ABP. As mentioned in Section 2.4, all measured waveforms were calibrated using values derived from brachial artery oscillometry, which estimated brachial SBP and DBP. Inverting equation (2.11) used to calculate MP, brachial SBP was individually estimated from MP and DBP of brachial PVR of each subject. Therefore the optimization problem for identifying the SLS model was formulated as the following.

$$\Theta_{SLS}^* = \arg \min_{\Theta_{SLS}} [|SP_B - \max(\hat{P}_B)| + |MP_B - \text{mean}(\hat{P}_B)| + |DP_B - \min(\hat{P}_B)|] \quad (4.7)$$

with constraints

$$E_{1B} > 0.0001, \quad E_{2B} > 0.0001, \quad \eta_B > 0.0001$$

where $\Theta_{SLS} = \{E_{1B}, E_{2B}, \eta_B\}$.

Then the SLS model equipped with Θ_{SLS}^* was used to estimate brachial ABP waveform, which was applied to the two-channel model along with an ankle PVR

waveform. The two-channel model was realized by minimizing the following optimization problem.

$$\Theta^* = \arg \min_{\Theta} \sqrt{\frac{1}{N} \sum_{k=1}^N [\hat{P}_{P,B}(k) - \hat{P}_{P,A}(k, \Theta)]^2} \quad (4.8)$$

with constraints

$$0.11 > \tau_B > 0.004, \quad 500 > \theta_{1B} > \theta_{2B} > 0.01, \quad 500 > \theta_{1A} > \theta_{2A} > 0.01$$

Afterwards, $\hat{P}_{P,B}$ and $\hat{P}_{P,A}$ were calculated using Θ^* and estimated central ABP was calculated as an average of both estimated central ABP waveforms.: $\hat{P}_P = 0.5\hat{P}_{P,B} + 0.5\hat{P}_{P,A}$.

The optimization was performed by scanning τ_B and optimizing the model for each fixed value of τ_B . Then by comparing the output of the objective function and τ_B , the optimal τ_B was selected as the point where the objective function output was minimal. In the optimization, a set of 21 initial conditions were used for each iteration of τ_B . Consequently, some of the optimized parameter values were very close to the prescribed boundaries. Such results were treated as numerical saturation of parameters and were excluded from the final results even if only one parameter was saturated.

4.6 Data Sets

For this study, 100 subjects were randomly selected from the same set of data obtained in a previous study [70]. The selected subject data files contained both brachial and ankle PVR waveforms as well as a carotid tonometry waveform to be used as a surrogate of central ABP waveform in evaluating the model results. In addition, conditions 1 and 2 listed in Section 2.4 needed to be satisfied. In preparation for the

system identification process the data were prepared in the same manner as in Chapter 2. The set of 100 subjects was separated into a testing set (n=50) and validation set (n=50).

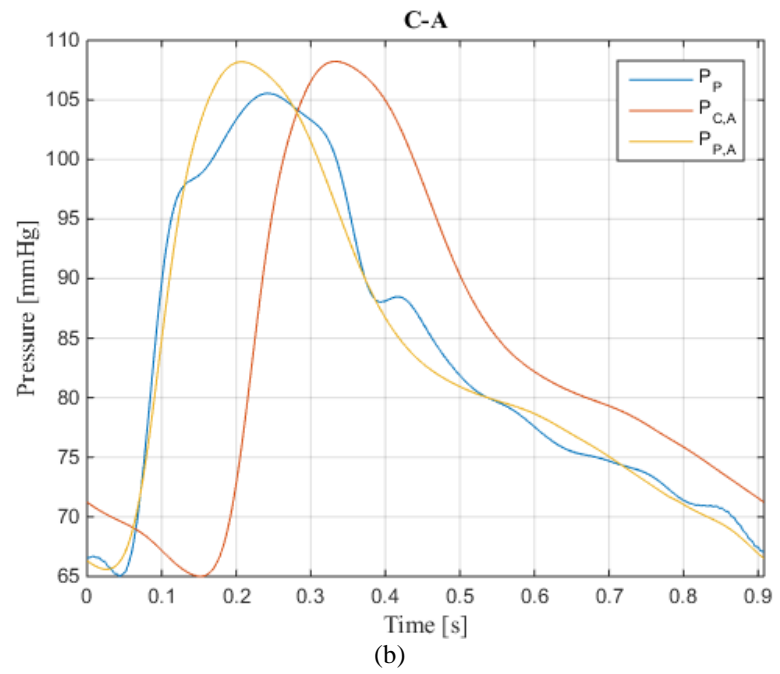
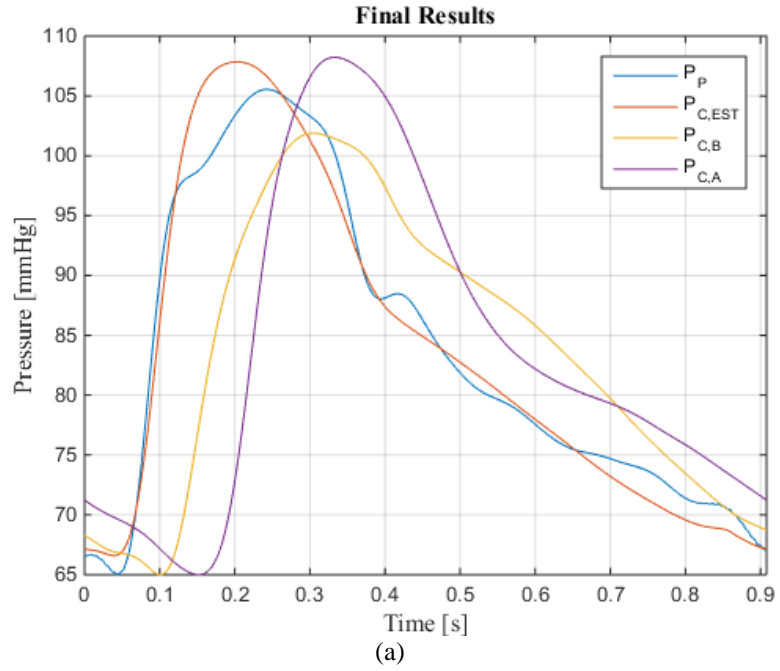
Table 4.1: Blind model identification subject characteristics

Characteristics	Median (IQR)
Male, %	55
Age	55 (47~69)
Carotid SBP (mmHg)	120.5 (104.1~131.7)
Carotid DBP (mmHg)	78 (67~88)
Carotid PP (mmHg)	41.5 (33.2~48.6)
Brachial Cuff SBP (mmHg)	113.9 (101.4~127.6)
Brachial Cuff DBP (mmHg)	78 (67~88)
Brachial Cuff PP (mmHg)	36.5 (29.7~42.7)
Ankle Cuff SBP (mmHg)	126.6 (112.8~139.4)
Ankle Cuff DBP (mmHg)	78 (67~88)
Ankle Cuff PP (mmHg)	47.0 (41.5~56.5)

4.7 Results

4.6.1 Model Selection (Testing Set)

An example of optimization results of (4.8) are presented below (Fig. 4.3). As shown in Fig. 4.3(a) the SBP and DBP errors between P_P and \hat{P}_C (labeled as $P_{C,EST}$ in the legend) was large.



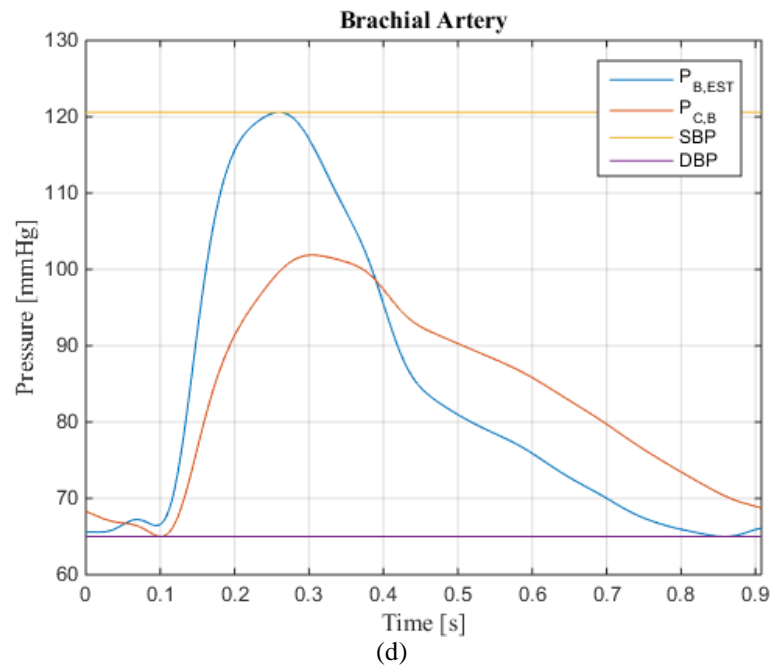
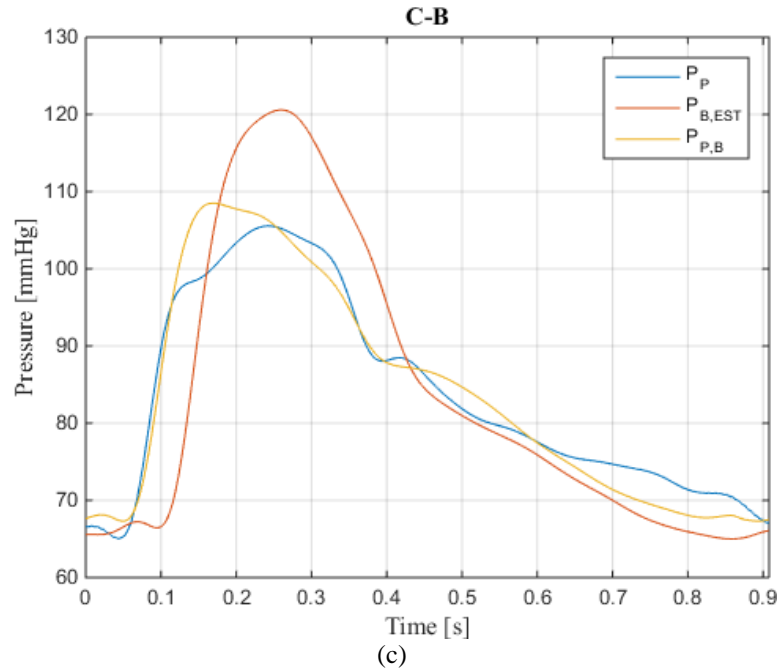


Fig. 4.3: Representative result of (4.8). (a) Overall results. (b) Carotid-posterior-tibial arterial path results. (c) carotid-brachial arterial path results. (d) SLS model results.

To test the hypothesis that improving DBP error will also indirectly improve SBP, DBP error was introduced into the objective function (4.8) in various forms (Table 4.2).

DBP error was defined as the difference between measured DBP, also used in SLS model optimization, and DBP of estimated central ABP waveform.

Table 4.2: Objective functions tested to reduce DBP error

Objective Functions	
1	$\min_{\Theta} \sqrt{\frac{1}{N} \sum_{k=1}^N [\hat{P}_{P,B}(k) - \hat{P}_{P,A}(k, \Theta)]^2}$
2	$\min_{\Theta} \left\{ \sqrt{\frac{1}{N} \sum_{k=1}^N [\hat{P}_{P,B}(k) - \hat{P}_{P,A}(k, \Theta)]^2} + DP_B - \min(\hat{P}_{P,B}) + DP_B - \min(\hat{P}_{P,A}) \right\}$
3	$\min_{\Theta} \left\{ \sqrt{\frac{1}{N} \sum_{k=1}^N [\hat{P}_{P,B}(k) - \hat{P}_{P,A}(k, \Theta)]^2} + 2 DP_B - \min(\hat{P}_{P,B}) + DP_B - \min(\hat{P}_{P,A}) \right\}$
4	$\min_{\Theta} \left\{ \sqrt{\frac{1}{N} \sum_{k=1}^N [\hat{P}_{P,B}(k) - \hat{P}_{P,A}(k, \Theta)]^2} + DP_B - \min(\hat{P}_{P,B}) \right\}$
5	$\min_{\Theta} \left\{ \sqrt{\frac{1}{N} \sum_{k=1}^N [\hat{P}_{P,B}(k) - \hat{P}_{P,A}(k, \Theta)]^2} + 2 DP_B - \min(\hat{P}_{P,B}) \right\}$
6	$\min_{\Theta} \left\{ \sqrt{\frac{1}{N} \sum_{k=1}^N [\hat{P}_{P,B}(k) - \hat{P}_{P,A}(k, \Theta)]^2} + DP_B - \min(\hat{P}_{P,A}) \right\}$
7	$\min_{\Theta} \left\{ \sqrt{\frac{1}{N} \sum_{k=1}^N [\hat{P}_{P,B}(k) - \hat{P}_{P,A}(k, \Theta)]^2} + 2 DP_B - \min(\hat{P}_{P,A}) \right\}$

However, it increased the number of subjects in which at least parameter was saturated for all 21 initial conditions. Additionally as shown in Table 4.3, the DP error was not significantly reduced.

Table 4.3: DP error incorporation results

Objective Function	# of unsaturated results	RMSE	SBP error	MP error	DBP error	PP error
1	50	3.56 (3.14~4.86)	-5.22 (-7.67~-3.00)	-0.01 (-0.04~0.05)	-0.92 (-1.7~-0.67)	-3.97 (-6.64~-1.57)
2	32	3.77 (3.11~4.81)	-5.73 (-7.75~-3.74)	-0.01 (-0.03~0.06)	-0.80 (-1.29~-0.59)	-4.75 (-7.29~-2.73)
3	38	3.91 (3.22~4.97)	-6.17 (-8.29~-4.01)	-0.01 (-0.03~0.06)	-0.74 (-1.24~-0.61)	-5.51 (-7.55~-2.90)
4	47	3.79 (3.12~4.91)	-5.19 (-7.79~-3.26)	-0.01 (-0.03~0.06)	-0.84 (-1.70~-0.62)	-3.97 (-6.88~-1.84)
5	47	3.98 (3.13~4.94)	-5.28 (-7.69~-3.45)	-0.01 (-0.03~0.06)	-0.83 (-1.81~-0.66)	-3.86 (-6.56~-1.69)
6	28	3.73 (3.26~5.08)	-6.11 (-7.82~-4.19)	-0.02 (-0.07~0.04)	-1.01 (-1.49~-0.63)	-4.69 (-6.97~-2.67)
7	19	3.77 (3.23~4.46)	-5.63 (-7.08~-4.53)	-0.01 (-0.03~0.06)	-0.91 (-1.37~-0.64)	-4.54 (-6.18~-3.38)

Due to the alarming number of saturated cases, a different approach was taken by incorporating SBP and PP error between $\hat{P}_{P,B}$ and $\hat{P}_{P,A}$. The new set of objective functions tested is listed in Table 4.4.

It is also important to note that the optimization ideally resulted in 21 results for each iterative value of τ_B . As a result, for each value of τ_B , the point in the parameter space that produced the smaller objective function value was selected as a candidate optimal point. However, some outliers would result in extremely small objective values and subsequently be selected as the optimal set of parameters. Therefore, the assumption that the most frequently occurring result is the desired local minimum for each value of τ_B was made, and it was applied by using the result closest to the median of the 21 results.

Table 4.4: Final set of candidate objective functions

Model Name	Objective Function
ITF-1	$\min_{\theta} \sqrt{\frac{1}{N} \sum_{k=1}^N [\hat{P}_{P,B}(k) - \hat{P}_{P,A}(k, \theta)]^2}$
ITF-2	$\min_{\theta} \left\{ \sqrt{\frac{1}{N} \sum_{k=1}^N [\hat{P}_{P,B}(k) - \hat{P}_{P,A}(k, \theta)]^2} + \max(\hat{P}_{P,B}) - \max(\hat{P}_{P,A}) \right\}$
ITF-3	$\min_{\theta} \left\{ \sqrt{\frac{1}{N} \sum_{k=1}^N [\hat{P}_{P,B}(k) - \hat{P}_{P,A}(k, \theta)]^2} + \max(\hat{P}_{P,B}) - \min(\hat{P}_{P,B}) - \max(\hat{P}_{P,A}) + \min(\hat{P}_{P,A}) \right\}$
ITF-4	$\min_{\theta} \left\{ \sqrt{\frac{1}{N} \sum_{k=1}^N [\hat{P}_{P,B}(k) - \hat{P}_{P,A}(k, \theta)]^2} + \max(\hat{P}_{P,B}) - \max(\hat{P}_{P,A}) + \max(\hat{P}_{P,B}) - \min(\hat{P}_{P,B}) - \max(\hat{P}_{P,A}) + \min(\hat{P}_{P,A}) \right\}$

The optimization results, both comparisons with P_p and average parameter values, are presented in Tables 4.5 and 4.6, respectively. The results suggest that ITF-4 may be the best suited out of the tested objective functions to relate ankle PVR and brachial PVR to the central ABP waveform. Although DBP error was not significantly different from that of ITF-1, shape error (RMSE), SBP error, and PP error were all improved significantly.

Identifiability conditions were satisfied as shown in Table 4.6. τ_B was large enough to satisfy $\tau_B F_S > 1$ and since δ_{Δ} was always positive, $\tau_A F_S > 1$ was always satisfied as well. Additionally, load parameter values, θ , for the two channels were different from each other avoiding pole-zero cancellations. Individual parameter results can be found in Table A1 in the Appendix.

Table 4.5: Results of final candidate objective functions. (Median(IQR))

Model	RMSE	SBP error	DBP error	PP error
ITF-1	3.55 (2.74~4.48)	-5.03 (-6.86~-2.15)	-0.94 (-1.53~-0.61)	-3.15 (-5.69~-1.36)
ITF-2	3.19 (2.32~4.06)*	-2.87 (-6.65~-0.69)	-0.84 (-1.37~-0.58)*	-2.18 (-5.54~-0.13)
ITF-3	3.14 (2.58~4.52)*†	-3.94 (-6.64~-1.25)†	-0.74 (-1.42~-0.56)*	-2.83 (-6.19~-0.58)†
ITF-4	3.08 (2.24~3.98)*†	-2.50 (-5.26~0.64)*†‡	-1.04 (-1.58~-0.70)	-1.48 (-4.25~1.72)*†‡

* : p<0.008 when compared to ITF-1

† : p<0.008 when compared to ITF-2

‡ : p<0.008 when compared to ITF-3

Table 4.6: Verification of identifiability conditions (testing set)

Model	τ_B [s]	θ_{1B} [s ⁻¹]	θ_{2B} [s ⁻¹]	θ_{1A} [s ⁻¹]	θ_{2A} [s ⁻¹]
ITF-1	0.034 (0.026~0.052)	40.7 (14.6~263.4)	38.8 (14.4~149.0)	4.26 (0.21~58.81)	0.88 (0.13~2.60)
ITF-2	0.032 (0.025~0.051)	19.2 (11.3~36.3)	16.9 (8.8~29.4)	58.2 (7.1~134.9)	1.28 (0.17~2.76)
ITF-3	0.036 (0.028~0.052)	22.7 (8.64~114.4)	17.4 (8.4~46.6)	48.0 (8.0~152.7)	1.19 (0.25~3.00)
ITF-4	0.036 (0.028~0.052)	14.4 (9.9~25.1)	13.9 (9.3~22.8)	308.2 (221.4~313.3)	17.8 (3.6~33.8)

ITF-4 was selected to evaluate its performance by comparison with the current standard of estimating central ABP waveform from PVR measurements. The current practice considers brachial PVR as a surrogate of central ABP waveform. Similarly ankle PVR was used as another proxy of central ABP waveform. Another common practice as mentioned in Section 1.4.1 and Table 1.1 is to apply a GTF to brachial PVR to estimate central ABP waveform, considering brachial PVR as a stand-in for brachial ABP waveform. Therefore, TLG model was applied to brachial PVR of the testing set, and the median values of the resulting optimal parameters were used to equip TLG-GTF to be evaluated with the validation set.

4.6.3 Comparison with State-of-the-Art (Validation Set)

ITF-4 and was applied to a new set of 50 subjects to compare its performance to current methods. ITF-4 better related brachial and ankle PVR to central ABP according to

the four metrics presented in Table 4.7. However, the DBP error for ankle and brachial PVR may be misleading. Since carotid tonometry, ankle, and brachial PVR were all calibrated to the same DBP, the DBP error will always be zero for this method. Interestingly, TLG-GTF outperformed ITF-4 in estimating SBP, DBP, and PP.

Table 4.7: Comparison of ITF-4 and current standards on validation set

Model	RMSE	SBP error	DBP error	PP error
ITF-4	3.08 (2.24~3.98)	-2.50 (-5.26~0.64)	-1.04 (-1.58~-0.70)	-1.48 (-4.25~1.72)
TLG-GTF	3.63 (2.63~4.59)	2.38 (-1.06~4.61)*	2.73 (2.43~3.06)*	-0.33 (-3.57~1.59)*
Ankle PVR	4.04 (3.02~6.35)*	-5.46 (-9.49~-2.75)*	0 (0~0)*	-5.46 (-9.49~-2.75)*
Brachial PVR	2.89 (2.08~4.36)*	4.58 (1.87~8.06)*	0 (0~0)*	4.58 (1.87~8.06)*

*: $p < 0.05$ when compared to ITF-4

Table 4.8: Verification of identifiability conditions (validation set)

τ_B [s]	θ_{1B} [s ⁻¹]	θ_{2B} [s ⁻¹]	θ_{1A} [s ⁻¹]	θ_{2A} [s ⁻¹]
0.038 (0.028~0.048)	12.59 (7.64~25.5)	12.1 (7.44~18.5)	305.4 (210.6~312.1)	22.1 (6.79~40.2)

The identifiability conditions were satisfied, as shown in Table 4.8. Load parameters associated with the carotid-brachial arterial path and carotid-posterior-tibial arterial path were distinct, avoiding pole-zero cancellation. In addition, τ_B and τ_A were sufficiently large to satisfy the blind identifiability condition. The individual results associated with each patient is presented in Table A2 in the Appendix.

4.8 Discussion

Pulse volume recordings are becoming increasingly popular in clinical settings due to its morphological similarity to ABP waveforms as well as their ease of use relative to risky methods such as catheterization or specialized techniques like applanation tonometry. However, it not a good surrogate of central ABP, and techniques such as GTFs have been developed to estimate central ABP. While GTFs offer valuable

information, they inherently lack the ability to account for inter-subject variability. As a result, a two-channel ITF was developed to estimate central ABP from two peripheral ABP measurements [55]. This study aimed to improve the model in order to apply it to PVR measurements that were shown to require additional complexity to compensate for viscoelastic effects of the arterial vessel, tissue, and BP cuff bladder, as discussed in Chapter 2.

Using the testing data a model, ITF-4, was shown to be most effective at achieving the objective. However comparisons with current methods using the validation set have shown that there is room for improvement. ITF-4 was better than brachial and ankle PVR, but this is a trivial conclusion as it has already been shown that peripheral PVR is not a great replacement for central ABP. Therefore, adjustments may need to be made to ITF in order to truly improve on the current gold standard.

Chapter 5: Conclusions and Future Directions

In Chapter 1, an exhaustive variety of transfer functions were tested in order to model the viscoelastic properties of the arterial wall, tissue, and BP cuff. Unlike the carotid-posterior-tibial arterial path which displayed little variance across the three transfer functions, the carotid-brachial arterial path may be better modeled by more complex viscoelastic models.

A broader inspection of the optimal ITF load parameters, from blind identification, shows that across all 100 subjects and across different ITF objective functions, the parameters τ_B , θ_{1B} , and θ_{2B} exhibited very little variance. Conversely, the parameters θ_{1A} and θ_{2A} were largely different between ITF-4 and the other ITF variations. This suggests that the model is more sensitive to τ_B , θ_{1B} , and θ_{2B} than θ_{1A} and θ_{2A} . A conjecture on the sensitivity of SLS parameters cannot be made because the ITF variations only applied to the objective function associated with the 2-channel model component. In other words the optimal SLS parameters were the same for a specific subject regardless of ITF variations.

Additionally, the similarity in the range of values of τ_B , θ_{1B} , and θ_{2B} suggest that these parameters may be fixed quantities, minimizing unnecessary computation time. Coupled with the fact that TLG-GTF outperformed ITF-4, an explicit parameter sensitivity analysis should be performed to find the minimum number of parameters required to optimally estimate central ABP from brachial and ankle PVR waveforms. That is, there may exist an optimal transfer function that is partly generalized and partly individualized.

Another possible explanation for the ITF inability to outperform TLG-GTF may be subtle differences in the data. For example if the ratio $\frac{SP}{MP}$ of a subject is large, it suggest that the waveform contains a relatively sharply shaped, high amplitude peak. Whereas if the ratio is large, then the waveform might be dull and short in amplitude. It may be interesting to investigate if ITF works better than GTF for subjects with a large $\frac{SP}{MP}$, or another ratio.

The ultimate goal of wave decomposition, discussed in Chapter 3, is to apply the technique to estimated central ABP waveform and estimated peripheral ABP waveforms resulting from two-sensor blind identification. The findings from Chapter 3 show that the technique may be further improved by optimizing tunable parameters in the model. Once optimized, application of wave decomposition to blind identification results may offer access to CV health risk factors that could be easily and quickly calculated from commonly accessible devices such as oscillometry devices.

Appendix

Table A1: Individual results for test set. (a) ITF-1. (b) ITF-2. (c) ITF-3. (d) ITF-4.

Subject ID	τ_B [s]	θ_{1B} [s ⁻¹]	θ_{2B} [s ⁻¹]	η_B [s]	E_{1B} [AU]	E_{2B} [AU]	τ_A [s]	θ_{1A} [s ⁻¹]	θ_{2A} [s ⁻¹]
C010203a	0.020	21.434	21.267	0.202	0.544	1.301	0.132	0.128	0.045
C010204a	0.012	28.041	27.824	0.249	0.315	2.227	0.084	0.098	0.097
C010204b	0.048	5.071	5.032	0.258	0.338	1.723	0.116	0.199	0.198
C010303b	0.052	3.042	1.394	0.192	0.444	1.248	0.132	94.117	10.352
C010405a	0.032	298.163	201.947	0.085	0.638	2.021	0.116	15.338	5.071
C010604b	0.036	4.453	4.418	0.240	0.495	1.350	0.124	45.715	2.025
C010705a	0.056	3.989	3.958	0.270	0.311	1.768	0.128	0.159	0.158
C010904a	0.020	24.567	24.376	0.214	0.195	2.672	0.104	0.098	0.097
C011305a	0.040	253.293	246.729	0.183	0.196	2.403	0.152	4.137	1.849
C011306a	0.032	4.166	4.134	0.314	0.310	1.384	0.108	44.467	4.446
C011405a	0.056	357.000	143.096	0.255	0.310	1.693	0.144	4.066	0.991
C011504a	0.064	376.392	123.633	0.265	0.328	1.371	0.148	0.408	0.405
C011604a	0.056	254.066	245.950	0.243	0.211	2.246	0.124	0.494	0.057
C011706a	0.048	287.510	212.546	0.104	0.750	0.948	0.144	1.730	0.854
C011805a	0.040	346.488	153.543	0.232	0.355	1.367	0.120	69.813	3.044
C012004a	0.072	186.432	63.839	0.223	0.302	1.393	0.196	21.994	2.179
C012105b	0.032	21.773	15.965	0.378	0.307	1.455	0.112	473.537	26.510
C012704a	0.016	38.688	38.388	0.180	0.543	1.347	0.120	480.464	19.595
C012705a	0.064	350.404	149.622	0.239	0.306	1.601	0.148	0.658	0.653
C012904a	0.040	251.547	248.478	0.276	0.500	1.256	0.104	342.464	1.693
C013004a	0.020	21.408	20.493	0.224	0.235	1.642	0.124	2.393	0.909
C013004b	0.032	4.518	4.483	0.218	0.357	1.861	0.124	60.719	0.037
C021204a	0.028	14.073	13.963	0.255	0.341	1.483	0.100	0.135	0.063
C021505a	0.056	319.015	181.153	0.195	0.237	1.575	0.132	4.383	1.236
C021704b	0.020	8.996	8.024	0.215	0.410	1.105	0.128	1.970	0.144
C021705a	0.072	5.106	5.066	0.306	0.332	2.115	0.136	0.234	0.232
C021904a	0.092	387.460	112.581	0.200	0.293	1.566	0.132	0.707	0.701
C022404a	0.048	314.690	185.333	0.231	0.330	1.480	0.108	95.359	0.166
C030105a	0.036	2.709	2.688	0.274	0.383	1.343	0.120	107.515	9.303
C030204b	0.028	10.804	10.720	0.208	0.498	1.493	0.140	80.398	4.161
C030405a	0.012	20.263	20.106	0.285	0.325	1.614	0.096	0.161	0.009
C030805a	0.032	266.541	233.502	0.187	0.303	1.857	0.124	12.232	2.190
C031105a	0.040	157.910	79.745	0.164	0.604	1.697	0.156	20.237	3.731
C031204a	0.024	20.076	19.920	0.269	0.345	1.459	0.100	0.079	0.078

C031505a	0.052	338.155	161.875	0.216	0.299	2.009	0.140	0.142	0.119
C031604a	0.060	101.970	54.312	0.221	0.175	2.878	0.140	0.138	0.069
C031904a	0.028	6.752	6.699	0.285	0.084	1.904	0.092	70.943	0.289
C031904b	0.032	168.368	152.075	0.155	0.550	3.017	0.140	1.186	0.572
C032504a	0.060	3.249	3.224	0.251	0.332	1.937	0.144	0.647	0.642
C033105a	0.028	22.042	19.655	0.209	0.447	1.454	0.116	0.138	0.015
C040805a	0.024	142.387	48.857	0.169	0.340	1.566	0.100	5.881	1.764
C040904a	0.008	16.024	15.899	0.262	0.336	1.731	0.104	0.098	0.097
C041205a	0.016	29.518	29.289	0.187	0.482	2.094	0.100	0.129	0.055
C041405a	0.052	338.108	161.939	0.279	0.095	2.052	0.144	53.096	2.730
C041505a	0.020	42.745	39.138	0.213	0.328	1.869	0.100	471.130	28.964
C041604a	0.036	223.663	123.952	0.148	0.555	2.254	0.156	9.455	1.376
C041905a	0.028	33.409	30.801	0.121	0.507	3.601	0.140	6.634	2.167
C042004a	0.040	352.857	147.194	0.268	0.340	1.431	0.124	317.322	1.446
C042205a	0.032	159.882	146.162	0.154	0.647	1.548	0.124	484.096	15.958
C042605a	0.028	142.657	129.676	0.176	0.325	2.475	0.128	14.723	4.576

(a)

Subject ID	τ_B [s]	θ_{1B} [s ⁻¹]	θ_{2B} [s ⁻¹]	η_B [s]	E_{1B} [AU]	E_{2B} [AU]	τ_A [s]	θ_{1A} [s ⁻¹]	θ_{2A} [s ⁻¹]
C010203a	0.036	26.396	17.598	0.202	0.544	1.301	0.148	109.452	0.023
C010204a	0.060	377.441	122.608	0.249	0.315	2.227	0.132	227.380	1.749
C010204b	0.052	6.019	5.972	0.258	0.338	1.723	0.120	383.331	3.454
C010303b	0.056	2.141	0.903	0.192	0.444	1.248	0.136	108.068	10.450
C010405a	0.024	28.989	28.764	0.085	0.638	2.021	0.108	11.334	4.244
C010604b	0.036	4.230	4.197	0.240	0.495	1.350	0.124	39.382	1.528
C010705a	0.052	4.203	4.170	0.270	0.311	1.768	0.124	55.987	0.108
C010904a	0.032	28.029	18.100	0.214	0.195	2.672	0.116	66.783	0.226
C011305a	0.032	16.854	16.723	0.183	0.196	2.403	0.144	4.121	1.888
C011306a	0.024	4.937	4.898	0.314	0.310	1.384	0.100	59.137	5.248
C011405a	0.032	16.197	15.051	0.255	0.310	1.693	0.120	1.972	1.039
C011504a	0.060	161.868	65.167	0.265	0.328	1.371	0.144	120.308	1.181
C011604a	0.044	12.163	12.068	0.243	0.211	2.246	0.112	315.952	2.641
C011706a	0.048	56.404	40.780	0.104	0.750	0.948	0.144	1.198	0.821
C011805a	0.024	16.624	16.495	0.232	0.355	1.367	0.104	23.900	1.230
C012004a	0.032	8.515	8.449	0.223	0.302	1.393	0.156	6.545	1.341
C012105b	0.024	19.236	17.053	0.378	0.307	1.455	0.104	99.277	0.024
C012704a	0.016	32.760	32.506	0.180	0.543	1.347	0.120	314.440	10.689
C012705a	0.064	112.792	60.066	0.239	0.306	1.601	0.148	281.671	2.378
C012904a	0.040	17.409	17.274	0.276	0.500	1.256	0.104	139.781	0.024
C013004a	0.020	15.910	15.787	0.224	0.235	1.642	0.124	4.737	1.058
C013004b	0.032	4.155	4.123	0.218	0.357	1.861	0.124	55.581	0.815

C021204a	0.048	23.079	16.626	0.255	0.341	1.483	0.120	147.698	2.096
C021505a	0.056	138.385	76.822	0.195	0.237	1.575	0.132	4.645	1.315
C021704b	0.020	11.204	8.066	0.215	0.410	1.105	0.128	0.191	0.149
C021705a	0.072	5.834	5.789	0.306	0.332	2.115	0.136	37.589	0.017
C021904a	0.088	376.665	123.161	0.200	0.293	1.566	0.128	57.889	0.035
C022404a	0.044	39.604	23.534	0.231	0.330	1.480	0.104	245.507	0.992
C030105a	0.028	2.505	2.486	0.274	0.383	1.343	0.112	106.500	9.517
C030204b	0.032	10.987	9.673	0.208	0.498	1.493	0.144	106.503	6.551
C030405a	0.048	31.727	16.736	0.285	0.325	1.614	0.132	82.783	0.020
C030805a	0.024	29.862	29.631	0.187	0.303	1.857	0.116	7.529	2.157
C031105a	0.028	21.963	20.194	0.164	0.604	1.697	0.144	15.583	3.115
C031204a	0.032	11.555	11.465	0.269	0.345	1.459	0.108	0.251	0.011
C031505a	0.060	348.730	151.302	0.216	0.299	2.009	0.148	98.675	0.904
C031604a	0.048	7.728	7.668	0.221	0.175	2.878	0.128	56.165	2.799
C031904a	0.024	6.964	6.910	0.285	0.084	1.904	0.088	108.788	0.178
C031904b	0.028	19.258	19.109	0.155	0.550	3.017	0.136	0.648	0.643
C032504a	0.060	11.696	5.614	0.251	0.332	1.937	0.144	0.209	0.020
C033105a	0.040	36.391	18.644	0.209	0.447	1.454	0.128	300.915	0.168
C040805a	0.024	189.893	55.306	0.169	0.340	1.566	0.100	5.946	1.928
C040904a	0.052	35.846	13.704	0.262	0.336	1.731	0.148	498.081	1.970
C041205a	0.028	16.816	16.686	0.187	0.482	2.094	0.112	58.414	0.011
C041405a	0.060	348.583	151.436	0.279	0.095	2.052	0.152	414.334	23.406
C041505a	0.020	23.293	23.112	0.213	0.328	1.869	0.100	261.989	15.106
C041604a	0.024	16.456	16.329	0.148	0.555	2.254	0.144	6.732	1.239
C041905a	0.028	17.995	17.855	0.121	0.507	3.601	0.140	6.984	2.234
C042004a	0.024	24.037	23.686	0.268	0.340	1.431	0.108	53.805	0.015
C042205a	0.036	216.988	161.155	0.154	0.647	1.548	0.128	489.003	10.973
C042605a	0.028	85.750	75.993	0.176	0.325	2.475	0.128	14.463	4.400

(b)

Subject ID	τ_B [s]	θ_{1B} [s ⁻¹]	θ_{2B} [s ⁻¹]	η_B [s]	E_{1B} [AU]	E_{2B} [AU]	τ_A [s]	θ_{1A} [s ⁻¹]	θ_{2A} [s ⁻¹]
C010203a	0.032	23.669	19.044	0.202	0.544	1.301	0.144	68.706	0.142
C010204a	0.028	17.409	17.273	0.249	0.315	2.227	0.100	30.601	0.014
C010204b	0.036	7.396	7.339	0.258	0.338	1.723	0.104	317.503	1.332
C010303b	0.056	3.837	0.846	0.192	0.444	1.248	0.136	259.680	24.662
C010405a	0.024	30.184	29.950	0.085	0.638	2.021	0.108	12.086	3.987
C010604b	0.036	4.451	4.417	0.240	0.495	1.350	0.124	55.690	2.617
C010705a	0.056	3.505	3.478	0.270	0.311	1.768	0.128	0.323	0.320
C010904a	0.044	128.133	48.450	0.214	0.195	2.672	0.128	147.016	0.043
C011305a	0.064	134.382	67.067	0.183	0.196	2.403	0.176	10.895	2.618
C011306a	0.032	3.828	3.799	0.314	0.310	1.384	0.108	40.237	4.420

C011405a	0.032	12.223	12.128	0.255	0.310	1.693	0.120	2.121	0.910
C011504a	0.060	94.711	30.815	0.265	0.328	1.371	0.144	0.339	0.336
C011604a	0.044	13.644	13.539	0.243	0.211	2.246	0.112	0.379	0.020
C011706a	0.036	22.906	22.129	0.104	0.750	0.948	0.132	0.660	0.655
C011805a	0.048	366.290	133.721	0.232	0.355	1.367	0.128	90.289	4.736
C012004a	0.072	192.806	67.536	0.223	0.302	1.393	0.196	31.510	3.118
C012105b	0.024	23.208	19.873	0.378	0.307	1.455	0.104	316.389	0.053
C012704a	0.016	37.741	37.448	0.180	0.543	1.347	0.120	340.266	13.609
C012705a	0.060	57.219	28.843	0.239	0.306	1.601	0.144	0.526	0.451
C012904a	0.036	15.750	15.628	0.276	0.500	1.256	0.100	152.932	0.069
C013004a	0.024	16.953	15.492	0.224	0.235	1.642	0.128	5.247	0.903
C013004b	0.028	4.527	4.492	0.218	0.357	1.861	0.120	56.927	0.775
C021204a	0.036	12.210	11.651	0.255	0.341	1.483	0.108	0.076	0.075
C021505a	0.060	311.944	188.182	0.195	0.237	1.575	0.136	12.407	1.342
C021704b	0.020	8.166	7.705	0.215	0.410	1.105	0.128	4.933	0.219
C021705a	0.072	6.425	6.375	0.306	0.332	2.115	0.136	29.979	0.232
C021904a	0.044	7.003	6.949	0.200	0.293	1.566	0.084	1.059	1.051
C022404a	0.052	190.941	90.274	0.231	0.330	1.480	0.112	151.084	0.959
C030105a	0.024	2.979	2.956	0.274	0.383	1.343	0.108	107.593	9.483
C030204b	0.028	10.079	10.001	0.208	0.498	1.493	0.140	56.557	2.042
C030405a	0.032	12.787	12.687	0.285	0.325	1.614	0.116	79.330	0.035
C030805a	0.028	41.471	41.150	0.187	0.303	1.857	0.120	9.807	1.799
C031105a	0.028	22.406	17.282	0.164	0.604	1.697	0.144	12.906	2.583
C031204a	0.048	33.730	16.480	0.269	0.345	1.459	0.124	386.029	0.563
C031505a	0.056	146.961	74.120	0.216	0.299	2.009	0.144	128.410	1.597
C031604a	0.052	7.931	7.843	0.221	0.175	2.878	0.132	30.922	2.115
C031904a	0.024	7.226	7.170	0.285	0.084	1.904	0.088	83.578	0.768
C031904b	0.048	230.822	128.482	0.155	0.550	3.017	0.156	313.586	7.001
C032504a	0.048	4.587	4.552	0.251	0.332	1.937	0.132	0.233	0.231
C033105a	0.052	358.875	131.893	0.209	0.447	1.454	0.140	398.438	4.216
C040805a	0.020	52.355	23.180	0.169	0.340	1.566	0.096	5.323	1.791
C040904a	0.032	14.080	13.868	0.262	0.336	1.731	0.128	152.154	0.042
C041205a	0.052	388.091	111.979	0.187	0.482	2.094	0.136	301.777	0.103
C041405a	0.060	350.598	149.250	0.279	0.095	2.052	0.152	227.320	13.143
C041505a	0.020	24.903	24.710	0.213	0.328	1.869	0.100	339.446	17.625
C041604a	0.028	18.199	17.580	0.148	0.555	2.254	0.148	9.887	1.435
C041905a	0.028	14.854	14.739	0.121	0.507	3.601	0.140	7.326	1.953
C042004a	0.024	32.835	29.863	0.268	0.340	1.431	0.108	345.269	0.737
C042205a	0.032	158.358	145.772	0.154	0.647	1.548	0.124	307.311	11.864
C042605a	0.028	121.015	111.622	0.176	0.325	2.475	0.128	15.124	4.764

(c)

Subject ID	τ_B [s]	θ_{1B} [s ⁻¹]	θ_{2B} [s ⁻¹]	η_B [s]	E_{1B} [AU]	E_{2B} [AU]	τ_A [s]	θ_{1A} [s ⁻¹]
C010203a	0.032	11.849	11.500	0.202	0.544	1.301	0.144	312.649
C010204a	0.028	9.253	9.181	0.249	0.315	2.227	0.100	313.347
C010204b	0.048	13.202	7.070	0.258	0.338	1.723	0.116	1.116
C010303b	0.052	4.103	0.845	0.192	0.444	1.248	0.132	304.658
C010405a	0.048	357.451	142.378	0.085	0.638	2.021	0.132	320.987
C010604b	0.032	8.896	7.824	0.240	0.495	1.350	0.120	314.198
C010705a	0.064	7.506	7.447	0.270	0.311	1.768	0.136	308.197
C010904a	0.028	25.749	21.068	0.214	0.195	2.672	0.112	110.047
C011305a	0.056	38.395	28.037	0.183	0.196	2.403	0.168	305.600
C011306a	0.024	18.255	11.233	0.314	0.310	1.384	0.100	313.078
C011405a	0.076	323.135	91.281	0.255	0.310	1.693	0.164	308.241
C011504a	0.036	13.562	13.457	0.265	0.328	1.371	0.120	45.980
C011604a	0.040	11.833	11.742	0.243	0.211	2.246	0.108	315.856
C011706a	0.040	16.134	16.009	0.104	0.750	0.948	0.136	2.598
C011805a	0.028	18.257	17.590	0.232	0.355	1.367	0.108	209.939
C012004a	0.064	245.660	89.040	0.223	0.302	1.393	0.188	323.260
C012105b	0.028	14.628	11.733	0.378	0.307	1.455	0.108	314.130
C012704a	0.016	23.216	23.010	0.180	0.543	1.347	0.120	312.014
C012705a	0.068	48.192	26.440	0.239	0.306	1.601	0.152	309.971
C012904a	0.040	14.399	14.288	0.276	0.500	1.256	0.104	263.997
C013004a	0.024	14.282	14.171	0.224	0.235	1.642	0.128	17.784
C013004b	0.036	5.833	5.788	0.218	0.357	1.861	0.128	311.854
C021204a	0.036	12.816	12.658	0.255	0.341	1.483	0.108	316.383
C021505a	0.036	17.040	16.908	0.195	0.237	1.575	0.112	4.450
C021704b	0.020	9.297	9.225	0.215	0.410	1.105	0.128	315.342
C021705a	0.072	6.549	6.499	0.306	0.332	2.115	0.136	316.381
C021904a	0.108	338.877	161.180	0.200	0.293	1.566	0.148	307.544
C022404a	0.040	13.730	13.624	0.231	0.330	1.480	0.100	255.973
C030105a	0.024	3.420	3.394	0.274	0.383	1.343	0.108	310.768
C030204b	0.028	9.355	9.282	0.208	0.498	1.493	0.140	314.395
C030405a	0.032	12.132	12.038	0.285	0.325	1.614	0.116	0.095
C030805a	0.024	22.341	22.167	0.187	0.303	1.857	0.116	307.959
C031105a	0.032	23.174	22.995	0.164	0.604	1.697	0.148	323.187
C031204a	0.032	10.939	10.854	0.269	0.345	1.459	0.108	0.241
C031505a	0.040	16.167	15.669	0.216	0.299	2.009	0.128	313.219
C031604a	0.052	9.589	9.515	0.221	0.175	2.878	0.132	209.361
C031904a	0.028	7.683	7.624	0.285	0.084	1.904	0.092	261.345
C031904b	0.064	117.785	50.995	0.155	0.550	3.017	0.172	312.096

C032504a	0.052	6.012	5.966	0.251	0.332	1.937	0.136	314.037	15.696
C033105a	0.028	14.494	14.377	0.209	0.447	1.454	0.116	75.511	2.030
C040805a	0.064	456.396	43.694	0.169	0.340	1.566	0.140	306.084	49.784
C040904a	0.036	9.394	9.183	0.262	0.336	1.731	0.132	56.251	3.456
C041205a	0.024	11.985	11.892	0.187	0.482	2.094	0.108	4.744	0.270
C041405a	0.036	15.996	15.872	0.279	0.095	2.052	0.128	304.610	20.498
C041505a	0.024	33.202	21.849	0.213	0.328	1.869	0.104	317.329	19.073
C041604a	0.056	127.328	57.790	0.148	0.555	2.254	0.176	309.896	41.953
C041905a	0.060	371.937	128.109	0.121	0.507	3.601	0.172	307.114	50.023
C042004a	0.028	13.092	12.990	0.268	0.340	1.431	0.112	310.521	27.841
C042205a	0.032	20.840	20.669	0.154	0.647	1.548	0.124	312.125	34.971
C042605a	0.040	50.057	24.701	0.176	0.325	2.475	0.140	295.177	110.776

(d)

Table A2: Individual results for ITF-4 on validation set

Subject ID	τ_B [s]	θ_{1B} [s ⁻¹]	θ_{2B} [s ⁻¹]	η_B [s]	E_{1B} [AU]	E_{2B} [AU]	τ_A [s]	θ_{1A} [s ⁻¹]	θ_{2A} [s ⁻¹]
C010203a	0.04	7.233	7.177	0.247	0.339	1.427	0.096	296.414	36.552
C010204a	0.04	9.347	9.274	0.245	0.295	2.154	0.148	0.245	0.243
C010204b	0.072	367.298	132.744	0.145	0.508	2.390	0.192	308.302	42.903
C010303b	0.032	10.851	10.767	0.227	0.366	2.162	0.116	0.185	0.105
C010405a	0.028	21.975	21.805	0.090	0.626	2.991	0.128	262.937	50.631
C010604b	0.032	2.175	2.158	0.230	0.353	1.336	0.128	54.253	13.361
C010705a	0.028	12.620	10.905	0.221	0.375	1.465	0.124	58.629	2.275
C010904a	0.036	13.313	12.191	0.245	0.325	1.741	0.108	56.472	2.072
C011305a	0.048	5.494	5.451	0.191	0.399	1.678	0.112	308.659	42.789
C011306a	0.056	3.438	3.411	0.334	0.340	1.511	0.136	249.700	28.275
C011405a	0.028	31.052	29.789	0.301	0.288	1.578	0.132	312.629	22.519
C011504a	0.036	12.560	10.424	0.223	0.327	2.162	0.112	56.107	6.198
C011604a	0.04	4.592	4.009	0.302	0.447	1.210	0.072	32.206	4.859
C011706a	0.032	10.727	9.815	0.284	0.098	2.414	0.112	314.124	8.557
C011805a	0.024	9.346	8.517	0.176	0.495	2.579	0.116	1.010	0.332
C012004a	0.02	26.300	24.904	0.158	0.297	3.321	0.108	312.996	19.255
C012105b	0.04	2.803	2.782	0.252	0.326	1.335	0.116	207.188	30.262
C012704a	0.04	3.482	3.455	0.479	0.290	1.491	0.156	309.891	35.503
C012705a	0.028	26.950	20.964	0.171	0.493	1.210	0.136	312.969	20.287
C012904a	0.036	23.256	19.600	0.216	0.336	1.726	0.112	307.781	40.845
C013004a	0.04	124.572	60.318	0.257	0.270	1.759	0.128	314.590	34.822
C013004b	0.04	22.330	22.157	0.179	0.190	2.814	0.120	312.554	37.157
C021204a	0.028	12.854	12.754	0.218	0.240	2.231	0.120	5.603	0.748
C021505a	0.028	317.444	182.610	0.143	0.486	1.539	0.104	291.784	43.739

C021704b	0.048	12.109	12.015	0.193	0.323	2.754	0.128	312.341	21.753
C021705a	0.044	18.325	18.183	0.206	0.259	1.967	0.132	305.238	59.594
C021904a	0.028	9.753	9.678	0.308	0.286	1.447	0.124	0.157	0.156
C022404a	0.02	40.926	40.608	0.126	0.355	1.613	0.092	311.399	38.086
C030105a	0.024	13.945	13.837	0.202	0.294	2.591	0.128	261.550	12.709
C030204b	0.104	221.744	218.862	0.274	0.231	0.723	0.104	258.512	241.564
C030405a	0.02	15.533	15.413	0.117	0.432	2.960	0.108	8.059	3.318
C030805a	0.02	12.236	12.141	0.307	0.293	1.245	0.088	314.104	8.839
C031105a	0.044	8.853	8.235	0.277	0.360	1.559	0.116	1.441	0.365
C031204a	0.06	3.980	3.949	0.299	0.310	1.778	0.136	309.206	41.102
C031505a	0.1	27.257	18.543	0.208	0.442	1.974	0.180	305.643	57.703
C031604a	0.036	11.206	11.119	0.208	0.355	1.609	0.128	315.050	8.925
C031904a	0.072	62.001	13.869	0.256	0.284	1.401	0.172	299.372	92.808
C031904b	0.04	9.423	9.350	0.253	0.363	1.835	0.164	314.976	18.912
C032504a	0.024	7.081	4.395	0.216	0.397	1.289	0.100	318.644	1.019
C033105a	0.048	43.893	16.609	0.148	0.742	0.941	0.156	220.933	15.307
C040805a	0.036	3.136	3.112	0.274	0.336	1.369	0.124	306.745	31.359
C040904a	0.056	12.131	12.037	0.206	0.189	3.248	0.160	310.843	30.411
C041205a	0.056	6.494	6.444	0.274	0.176	1.746	0.112	306.624	52.676
C041405a	0.028	23.278	16.418	0.209	0.262	1.985	0.124	313.026	21.383
C041505a	0.064	26.373	16.607	0.266	0.175	2.289	0.164	335.698	24.872
C041604a	0.036	17.707	17.570	0.208	0.366	2.053	0.136	310.800	30.971
C041905a	0.056	2.944	2.921	0.286	0.333	1.446	0.144	304.886	61.530
C042004a	0.052	46.466	37.100	0.147	0.527	1.757	0.128	260.778	19.528
C042205a	0.056	3.359	3.333	0.324	0.514	1.314	0.128	306.738	52.046
C042605a	0.02	14.244	14.129	0.245	0.264	1.985	0.088	262.632	0.117

Bibliography

- [1] D. Mozaffarian *et al.*, “Heart disease and stroke statistics-2016 update a report from the American Heart Association,” *Circulation*, vol. 133, no. 4, pp. 447–454, 2016.
- [2] N. Westerhof, P. Sipkema, G. C. Van Den Bos, and G. Elzinga, “Forward and backward waves in the arterial system,” *Cardiovasc. Res.*, vol. 6, no. 6, pp. 648–656, 1972.
- [3] A. Noordergraaf, *Circulatory System Dynamics*. New York: Academic Press, 1978.
- [4] W. W. Nichols, M. F. O’Rourke, and C. Vlachopoulos, *McDonald’s blood flow in arteries; theoretical, experimental and clinical principles*, 6th ed. CRC Press, 2011.
- [5] G. M. London and a P. Guerin, “Influence of arterial pulse and reflected waves on blood pressure and cardiac function.,” *Am. Heart J.*, vol. 138, no. 3 Pt 2, pp. 220–224, 1999.
- [6] Yasmin and M. J. Brown, “Similarities and differences between augmentation index and pulse wave velocity in the assessment of arterial stiffness.,” *QJM*, vol. 92, no. 10, pp. 595–600, 1999.
- [7] A. Qasem and A. Avolio, “Determination of Aortic Pulse Wave Velocity From Waveform Decomposition of the Central Aortic Pressure Pulse,” *Hypertension*, vol. 51, pp. 1–8, 2008.
- [8] G. F. Mitchell *et al.*, “Changes in arterial stiffness and wave reflection with advancing age in healthy men and women: the Framingham Heart Study.,” *Hypertension*, vol. 43, no. 6, pp. 1239–1245, 2004.
- [9] P. Segers *et al.*, “Noninvasive (Input) Impedance, Pulse Wave Velocity, and Wave Reflection in Healthy Middle-Aged Men and Women,” *Hypertension*, vol. 49, pp. 1248–1255, 2007.
- [10] K. L. Wang *et al.*, “Wave reflection and arterial stiffness in the prediction of 15-year all-cause and cardiovascular mortalities: a community-based study,” *Hypertension*, vol. 55, pp. 499–805, 2010.
- [11] E. P. Widmayer, H. Raff, and K. T. Strang, *Vander’s Human Physiology*, 12th ed., no. 1. McGraw Hill, 2010.
- [12] W. K. Laskey and W. G. Kussmaul, “Arterial wave reflection in heart failure.,” *Circulation*, vol. 75, no. 4, pp. 711–22, 1987.
- [13] Y. Matsui, K. Kario, J. Ishikawa, K. Eguchi, S. Hoshide, and K. Shimada, “Reproducibility of arterial stiffness indices (pulse wave velocity and augmentation index) simultaneously assessed by automated pulse wave analysis

- and their associated risk factors in essential hypertensive patients.,” *Hypertension Research*, vol. 27, no. 11, pp. 851–7, 2004.
- [14] F. van de Vosse and N. Stergiopoulos, “Pulse wave propagation in the arterial tree,” *Annual Review of Fluid Mechanics*, vol. 43, pp. 467–499, 2011.
- [15] M. E. Safar *et al.*, “Central pulse pressure and mortality in end-stage renal disease,” *Hypertension*, vol. 39, no. 3, pp. 735–738, 2002.
- [16] C. Lorenzo, K. Aung, M. P. Stern, and S. M. Haffner, “Pulse pressure, prehypertension, and mortality: the San Antonio heart study,” *American Journal of Hypertens*, vol. 22, no. 11, pp. 1219–1226, 2009.
- [17] F. Hadaegh, G. Shafiee, M. Hatami, and F. Azizi, “Systolic and diastolic blood pressure, mean arterial pressure and pulse pressure for prediction of cardiovascular events and mortality in a Middle Eastern population.,” *Blood Pressure*, vol. 21, no. 1, pp. 12–18, 2012.
- [18] L. N. Borrell and L. Samuel, “The effect of pulse pressure on all-cause and cardiovascular-specific mortality risks in us adults,” *Ethnicity & Disease*, vol. 25, no. 2, pp. 152–156, 2015.
- [19] C. J. Petrie, A. A. Voors, M. Robertson, D. J. Van Veldhuisen, and H. J. Dargie, “A low pulse pressure predicts mortality in subjects with heart failure after an acute myocardial infarction: A post-hoc analysis of the CAPRICORN study,” *Clinical Research in Cardiology*, vol. 101, no. 1, pp. 29–35, 2012.
- [20] A. Benetos *et al.*, “Mortality and Cardiovascular Events Are Best Predicted by Low Central/Peripheral Pulse Pressure Amplification But Not by High Blood Pressure Levels in Elderly Nursing Home Subjects: the PARTAGE (Predictive Values of Blood Pressure and Arterial Stiffness i,” *Journal of the American College of Cardiology*, vol. 60, no. 16, pp. 1503–1511, 2012.
- [21] B. E. Westerhof, I. Guelen, N. Westerhof, J. M. Karemaker, and A. Avolio, “Quantification of wave reflection in the human aorta from pressure alone: A proof of principle,” *Hypertension*, vol. 48, no. 4, pp. 595–601, 2006.
- [22] J. G. Kips *et al.*, “Evaluation of noninvasive methods to assess wave reflection and pulse transit time from the pressure waveform alone,” *Hypertension*, vol. 53, no. 2, pp. 142–149, 2009.
- [23] A. P. Avolio *et al.*, “Role of pulse pressure amplification in arterial hypertension: Experts’ opinion and review of the data,” *Hypertension*, vol. 54, no. 2, pp. 375–383, 2009.
- [24] T. K. Waddell, A. M. Dart, T. L. Medley, J. D. Cameron, and B. A. Kingwell, “Carotid pressure is a better predictor of coronary artery disease severity than brachial pressure.,” *Hypertension*, vol. 38, no. 4, pp. 927–31, 2001.

- [25] M. J. Roman *et al.*, “Central pressure more strongly relates to vascular disease and outcome than does brachial pressure: The strong heart study,” in *Hypertension*, vol. 50, no. 1, pp. 197–203, 2007.
- [26] R. Pini *et al.*, “Central But Not Brachial Blood Pressure Predicts Cardiovascular Events in an Unselected Geriatric Population. The ICARe Dicomano Study,” *Journal of the American College of Cardiology*, vol. 51, no. 25, pp. 2432–2439, 2008.
- [27] M. E. Safar and P. Jankowski, “Central blood pressure and hypertension: role in cardiovascular risk assessment.,” *Clinical Science*, vol. 116, no. 4, pp. 273–82, 2009.
- [28] I. B. Wilkinson, C. M. McEniery, and J. R. Cockcroft, “Central blood pressure estimation for the masses moves a step closer.,” *Journal of Human Hypertension*, vol. 24, no. 8, pp. 495–497, 2010.
- [29] T. G. Papaioannou, A. D. Protogerou, K. S. Stamatelopoulos, M. Vavuranakis, and C. Stefanadis, “Non-invasive methods and techniques for central blood pressure estimation: procedures, validation, reproducibility and limitations.,” *Current Pharmaceutical Design*, vol. 15, no. 3, pp. 245–253, 2009.
- [30] G. M. Drzewiecki, J. Melbin, and A. Noordergraaf, “Arterial tonometry: Review and analysis,” *Journal of Biomechanics*, vol. 16, no. 2, pp. 141–152, 1983.
- [31] R. P. Kelly, M. Karamanoglu, H. Gibbs, A. P. Avolio, and M. F. O’Rourke, “Noninvasive Carotid Pressure Wave registration as an indicator of ascending aortic pressure,” *Journal of Vascular Medicine and Biology*, vol. 1, pp. 241–247, 1989.
- [32] R. P. Kelly, C. Hayward, J. Ganis, J. Daley, A. Avolio, and M. F. O’Rourke, “Noninvasive registration of the arterial pressure pulse waveform; using high-fidelity applanation tonometry,” *Journal of Vascular Medicine and Biology*, vol. 1, pp. 142–149, 1989.
- [33] C. H. Chen *et al.*, “Validation of carotid artery tonometry as a means of estimating augmentation index of ascending aortic pressure,” *Hypertension*, vol. 27, no. 2, pp. 168–175, 1996.
- [34] R. E. Climie, M. G. Schultz, S. B. Nikolic, K. D. Ahuja, J. W. Fell, and J. E. Sharman, “Validity and reliability of central blood pressure estimated by upper arm oscillometric cuff pressure,” *American Journal of Hypertension*, vol. 25, no. 4, pp. 414–420, 2012.
- [35] Y. Watanabe *et al.*, “Ankle-Brachial Index, Toe-Brachial Index, and Pulse Volume Recording in Healthy Young Adults,” *Annals of Vascular Diseases*, vol. 8, no. 3, pp. 227–235, 2015.

- [36] J. E. Lewis, P. Williams, and J. H. Davies, “Non-invasive assessment of peripheral arterial disease: Automated ankle brachial index measurement and pulse volume analysis compared to duplex scan,” *SAGE Open Medicine*, vol. 4, no. 0, pp. 64–83, Jul. 2016.
- [37] W. J. Verberk, H. Cheng, L. Huang, C. Lin, Y. Teng, and C. Chen, “Practical Suitability of a Stand-Alone Oscillometric Central Blood Pressure Monitor : A Review of the Microlife WatchBP Office Central,” *Pulse (Basel)*, no. 431, pp. 205–216, 2016.
- [38] J. Liu *et al.*, “Patient-Specific Oscillometric Blood Pressure Measurement,” *IEEE Transactions on Biomedical Engineering*, vol. 9294, no. c, pp. 1–1, 2015.
- [39] P. K. Lim *et al.*, “Improved Measurement of Blood Pressure by Extraction of Characteristic Features from the Cuff Oscillometric Waveform,” *Sensors*, vol. 15, pp. 14142–14161, 2015.
- [40] M. Karamanoglu, M. F. O’Rourke, a P. Avolio, and R. P. Kelly, “An analysis of the relationship between central aortic and peripheral upper limb pressure waves in man.,” *European Heart Journal*, vol. 14, no. 2, pp. 160–167, 1993.
- [41] B. Fetcs, E. Nevo, C. H. Chen, and D. A. Kass, “Parametric model derivation of transfer function for noninvasive estimation of aortic pressure by radial tonometry,” *IEEE Transactions on Biomedical Engineering*, vol. 46, no. 6, pp. 698–706, 1999.
- [42] A. L. Pauca, M. F. O’Rourke, and N. D. Kon, “Prospective evaluation of a method for estimating ascending aortic pressure from the radial artery pressure waveform.,” *Hypertension*, vol. 38, no. 4, pp. 932–937, 2001.
- [43] S. Söderström, G. Nyberg, M. F. O’Rourke, J. Sellgren, and J. Pontén, “Can a clinically useful aortic pressure wave be derived from a radial pressure wave?,” *British Journal of Anaesthesia.*, vol. 88, no. 4, pp. 481–488, 2002.
- [44] D. Gallagher, A. Adji, and M. F. O’Rourke, “Validation of the transfer function technique for generating central from peripheral upper limb pressure waveform,” *American Journal of Hypertension*, vol. 17, pp. 1059–1067, 2004.
- [45] J. E. Sharman *et al.*, “Validation of a generalized transfer function to noninvasively derive central blood pressure during exercise,” *Hypertension*, vol. 47, no. 6, pp. 1203–1208, 2006.
- [46] H. M. Cheng *et al.*, “Estimation of central systolic blood pressure using an oscillometric blood pressure monitor.,” *Hypertension Research*, vol. 33, no. 6, pp. 592–9, 2010.
- [47] T. Weber *et al.*, “Validation of a brachial cuff-based method for estimating central systolic blood pressure,” *Hypertension*, vol. 58, no. 5, pp. 825–832, 2011.

- [48] Y. T. Shih, H. M. Cheng, S. H. Sung, W. C. Hu, and C. H. Chen, "Comparison of two generalized transfer functions for measuring central systolic blood pressure by an oscillometric blood pressure monitor.," *Journal of Human Hypertension*, vol. 27, no. 3, pp. 204–10, 2013.
- [49] G. Swamy, Q. Ling, T. Li, and R. Mukkamala, "Blind identification of the aortic pressure waveform from multiple peripheral artery pressure waveforms.," *American Journal of Physiology Heart and Circulatory Physiology*, vol. 292, no. 5, pp. H2257–64, 2007.
- [50] J.-O. Hahn, A. T. Reisner, and H. H. Asada, "Blind Identification of Two-Channel IIR Systems With Application to Central Cardiovascular Monitoring," *Journal of Dynamic Systems, Measurement, and Control*, vol. 131, no. September, p. 051009, 2009.
- [51] J.-O. Hahn, A. T. Reisner, and H. Harry Asada, "Modeling and 2-Sensor Blind Identification of Human Cardiovascular System," *Control Engineering Practice*, vol. 17, no. 11, pp. 1318–1328, 2009.
- [52] G. Swamy, D. Xu, N. B. Olivier, and R. Mukkamala, "An adaptive transfer function for deriving the aortic pressure waveform from a peripheral artery pressure waveform.," *American Journal of Physiology Heart and Circulatory Physiology*, vol. 297, no. 5, pp. H1956–H1963, 2009.
- [53] J. O. Hahn, A. T. Reisner, F. A. Jaffer, and H. H. Asada, "Subject-specific estimation of central aortic blood pressure using an individualized transfer function: A preliminary feasibility study," *IEEE Transactions on Information Technology in Biomedicine*, vol. 16, no. 2, pp. 212–220, 2012.
- [54] M. Rashedi *et al.*, "Comparative study on tube-load modeling of arterial hemodynamics in humans," *Journal Biomechanical Engineering*, vol. 135, no. 3, p. 31005, 2013.
- [55] N. Fazeli *et al.*, "Subject-specific estimation of central aortic blood pressure via system identification: preliminary in-human experimental study," *Medical & Biological Engineering & Computing*, vol. 52, no. 10, pp. 895–904, 2014.
- [56] M. Abdollahzade, C. S. Kim, N. Fazeli, B. A. Finegan, M. Sean McMurtry, and J. O. Hahn, "Data-driven lossy tube-load modeling of arterial tree: in-human study.," *Journal of Biomechanical Engineering*, vol. 136, no. 10, p. 101011, 2014.
- [57] S. Wassertheurer *et al.*, "A new oscillometric method for pulse wave analysis: comparison with a common tonometric method.," *Journal of Human Hypertension*, vol. 24, no. 8, pp. 498–504, 2010.
- [58] S. E. Brett, A. Guilcher, B. Clapp, and P. Chowienczyk, "Estimating central systolic blood pressure during oscillometric determination of blood pressure: proof of concept and validation by comparison with intra-aortic pressure recording and

- arterial tonometry,” *Blood Pressure Monitoring*, vol. 17, no. 3, pp. 132–136, 2012.
- [59] M. I. Güreli and C. L. Nikias, “EVAM: An Eigenvector-Based Algorithm for Multichannel Blind Deconvolution of Input Colored Signals,” *IEEE Transactions on Signal Processing*, vol. 43, no. 1, pp. 134–149, 1995.
- [60] G. Xu, H. Liu, L. Tong, and T. Kailath, “A least-squares approach to blind channel identification,” *IEEE Transactions on Signal Processing*, vol. 43, pp. 2982–2993, 1995.
- [61] D. L. Newman, S. E. Greenwald, and N. L. Bowden, “An in vivo study of the total occlusion method for the analysis of forward and backward pressure waves,” *Cardiovascular Research*, vol. 13, no. 10, pp. 595–600, 1979.
- [62] D. G. Edwards, C. R. Mastin, and R. W. Kenefick, “Wave reflection and central aortic pressure are increased in response to static and dynamic muscle contraction at comparable workloads,” *Journal of Applied Physiology*, vol. 104, pp. 439–445, 2008.
- [63] C. C. Lee and R. G. Mark, “Analysis of Arterial Waves by the Single-Pulse-Response Method,” *IEEE Transactions on Biomedical Engineering*, vol. 40, no. 8, pp. 833–836, 1993.
- [64] R. Burattini and K. B. Campbell, “Modified asymmetric T-tube model to infer arterial wave reflection at the aortic root,” *IEEE Transactions on Biomedical Engineering*, vol. 36, no. 8, pp. 805–814, 1989.
- [65] K. B. Campbell, R. Burattini, D. L. Bell, R. D. Kirkpatrick, and G. G. Knowlen, “Time-domain formulation of asymmetric T-tube model of arterial system,” *American Journal of Physiology*, vol. 258, no. 6 Pt 2, pp. H1761–H1774, 1990.
- [66] G. Swamy, N. B. Olivier, and R. Mukkamala, “Calculation of forward and backward arterial waves by analysis of two pressure waveforms,” *IEEE Transactions on Biomedical Engineering*, vol. 57, no. 12, pp. 2833–2839, 2010.
- [67] J. A. KONG, *Electromagnetic Wave Theory*. EMW Publishing, 1986.
- [68] G. Zhang, J. O. Hahn, and R. Mukkamala, “Tube-load model parameter estimation for monitoring arterial hemodynamics,” *Frontiers in Physiology*, vol. 2 NOV. pp. 1–18, 2011.
- [69] L. Lennart, *System identification: theory for the user (second edition)*, 2nd ed. Prentice Hall, 1999.
- [70] W.-C. Yu, S.-Y. Chuang, Y.-P. Lin, and C.-H. Chen, “Brachial-ankle vs carotid-femoral pulse wave velocity as a determinant of cardiovascular structure and function,” *Journal of Human Hypertension*, vol. 22, no. 1, pp. 24–31, 2008.

- [71] C. Kim, N. Fazeli, M. S. Mcmurtry, B. A. Finegan, and J. Hahn, “Quantification of Wave Reflection Using Peripheral Blood Pressure Waveforms,” *Journal of Biomedical and Health Informatics*, vol. 19, no. 1, pp. 309–316, 2015.
- [72] P. Segers *et al.*, “Individualizing the aorto-radial pressure transfer function: feasibility of a model-based approach.,” *American Journal of Physiology Heart and Circulatory Physiology*, vol. 279, no. 2, pp. H542–9, 2000.
- [73] P. Reymond, F. Merenda, F. Perren, D. Rüfenacht, and N. Stergiopoulos, “Validation of a one-dimensional model of the systemic arterial tree,” *American Journal of Physiology Heart and Circulatory Physiology*, vol. 297, no. 1, pp. H208–H222, 2009.